

# Tensile Strengths of Silicon Carbide (SiC) Under Shock Loading

by Dattatraya P. Dandekar and Peter T. Bartkowski

ARL-TR-2430

March 2001

Approved for public release; distribution is unlimited.

20010402 116

The findings in this report are not to be construed as an official Department of the Army position unless so designated by other authorized documents.

Citation of manufacturer's or trade names does not constitute an official endorsement or approval of the use thereof.

Destroy this report when it is no longer needed. Do not return it to the originator.

# Army Research Laboratory

Aberdeen Proving Ground, MD 21005-5066

---

---

ARL-TR-2430

March 2001

## Tensile Strengths of Silicon Carbide (SiC) Under Shock Loading

Dattatraya P. Dandekar and Peter T. Bartkowski  
Weapons and Materials Research Directorate, ARL

---

## Abstract

---

The present work was initiated to measure and compare tensile strengths (i.e., spall thresholds) of five different types/varieties of silicon carbide materials. Two of these materials were sintered, and the remaining three were hot-pressed. Three types of silicon carbides (one sintered by Sohio and the other two hot-pressed by Cercom) were manufactured in the United States. The remaining two varieties of silicon carbides were manufactured in France. Spall strengths of these five different silicon carbide materials were measured by performing plane shock wave experiments to a maximum impact-generated stress level of 17 GPa on the light gas-gun facility at the U.S. Army Research Laboratory (ARL). The single most important result of this investigation is that spall strength of silicon carbide, irrespective of its manufacturing process, improves initially to a certain impact stress level before it begins to deteriorate under higher impact stress. The decline in the spall strength of both sintered materials and Cercom SiC-B begin at an impact stress between 3–5 GPa. SiC-N data have a very large scatter. Spall strength of the French sintered and hot-pressed material increases to an impact stress of 11.7 GPa. Its spall strength increases from 0.8 GPa at an impact stress of 1.6 GPa to 1.8 GPa at an impact stress of 11.7 GPa. In terms of spall strength, the French sintered and hot-pressed materials show the least scatter and largest increase with an increase in the impact stress. The results of the present work thus offer new challenges to modeling ceramic materials.

# Table of Contents

	<u>Page</u>
<b>List of Figures</b> .....	v
<b>List of Tables</b> .....	vii
<b>1. Introduction</b> .....	1
<b>2. Materials</b> .....	2
2.1 U.S. Materials .....	2
2.1.1 <i>Sohio Material: Sintered SiC</i> .....	3
2.1.2 <i>Hot-Pressed SiC SiC-B</i> .....	3
2.1.3 <i>Hot-Pressed SiC SiC-N</i> .....	3
2.2 French SiC .....	4
<b>3. Material Properties</b> .....	4
3.1 Elemental Composition.....	4
3.2 Microstructure.....	4
3.3 Density and Elastic Constants.....	5
3.3.1 <i>Density</i> .....	8
3.3.2 <i>Elastic Constants</i> .....	9
<b>4. Design of Shock Experiments</b> .....	11
<b>5. Results</b> .....	13
5.1 Data Analysis .....	13
5.2 Results of Spall Experiments.....	19
5.2.1 <i>Sintered SiC</i> .....	19
5.2.2 <i>Hot-Pressed SiC</i> .....	21
5.2.2.1 <i>SiC-B</i> .....	25
5.2.2.2 <i>SiC-N</i> .....	25
5.2.3 <i>French Sintered and Hot-Pressed SiC</i> .....	26
5.2.4 <i>Summary</i> .....	30
5.2.4.1 <i>Spall Strength Variation Trend</i> .....	30
5.2.4.2 <i>Sohio Material</i> .....	30
5.2.4.3 <i>Spall Threshold Increase</i> .....	31
5.2.4.4 <i>Free-Surface Velocity Decline</i> .....	31

	<u>Page</u>
6. <b>Discussion</b> .....	31
7. <b>Future Work</b> .....	34
8. <b>References</b> .....	37
<b>Distribution List</b> .....	39
<b>Report Documentation Page</b> .....	45

## List of Figures

<u>Figure</u>	<u>Page</u>
1. Microphotograph of Sohio Sintered SiC.....	6
2. Microphotograph of French Sintered SiC.....	6
3. Microphotograph of Hot-Pressed SiC-B.....	7
4. Microphotograph of Hot-Pressed SiC-N.....	7
5. Microphotograph of French Sintered and Hot-Pressed SiC.....	8
6. Variation in Ultrasonic Wave Velocities as a Function of Density in SiC .....	10
7. Two Configurations of Symmetric Transmission Experiments With a PMMA Window and Without a PMMA Window.....	12
8. A Schematic of Stress vs. Particle Velocity for Shock, Release, and Tensile Paths in an Elastic-Plastic Material for Analyzing Wave Profile Data .....	13
9. Free-Surface Velocity in Profiles in SiC, Impact Velocity 0.08 km/s .....	15
10. Velocity Profiles in SiC, Impact Velocity 0.6 km/s.....	15
11. Spall Strength vs. Impact Stress of Sohio SiC.....	20
12. Spall Strength vs. Impact Stress of French Sintered SiC.....	21
13. Spall Strength vs. Impact Stress of SiC-B. ....	25
14. Spall Strength vs. Impact Stress of SiC-N.....	26
15. Free-Surface Velocity Profiles in SiC-N.....	27
16. Spall Strength vs. Impact Stress of French Sintered and Hot-Pressed SiC.....	29
17. Free-Surface Velocity Profiles in French Sintered and Hot-Pressed SiC .....	29
18. Spall Strength vs. Impact Stress of French Sintered and Hot-Isostatically-Pressed SiC and Hot-Pressed SiC .....	34

INTENTIONALLY LEFT BLANK.

## List of Tables

<u>Table</u>		<u>Page</u>
1.	Elemental Compositions of SiC Materials.....	5
2.	Density and Ultrasonic Wave Velocities of Five SiC Materials.....	8
3.	Elastic Constants of SiC Materials .....	10
4.	Data From Transmission Experiments on Sohio Sintered SiC.....	16
5.	Summary of the Results of Transmission Experiments on Sohio Sintered SiC. ....	16
6.	Data From Transmission Experiments on French Sintered SiC .....	17
7.	Summary of the Results of Transmission Experiments on French Sintered SiC.....	17
8.	Data From Transmission Experiments on SiC-B.....	18
9.	Summary of the Results of Transmission Experiments on SiC-B.....	22
10.	Data From Transmission Experiments on SiC-N. ....	23
11.	Summary of the Results of Transmission Experiments on SiC-N.....	24
12.	Data From Transmission Experiments on French Sintered and Hot-Pressed SiC.....	28
13.	Summary of the Results of Transmission Experiments on French Sintered and Hot-Pressed SiC.....	28

INTENTIONALLY LEFT BLANK.

# 1. Introduction

Materials play an important role in the design of an armor system. An advanced armor system is composed of a complex combination of different materials. These materials include ceramic, metal, and polymer matrix composites. The primary function of ceramic is to reduce/disintegrate the impacting projectile through rupture, blunting, and erosion. Ceramic materials are attractive because of their low density, high hardness, high elastic moduli, low compressibility, and good weathering and erosion resistance property. However, it is not yet clear what combination of mechanical and physical properties under a given geometrical configuration will make ceramics relatively impenetrable to a given projectile at a given impact velocity. However, since materials used in an armor system are subject to high strain rates of deformation at and around the impact locations, it is necessary to measure relevant mechanical and physical properties of the materials under similar loading conditions in the laboratory. In other words, experiments must be conducted to determine properties of the materials under well-defined impact conditions.

Under plane shock wave loading, the properties of a material under inertial confinement are measured under shock wave-induced stress and one-dimensional strain (1-D) in the direction of wave propagation. Thus, the properties of a material measured under plane shock wave loading reflect the best performance that the material is expected to display in an impact loading condition (in terms of its compressibility, shear strength, and tensile strength) because it is not influenced by the geometry of the material configuration. Earlier works on ceramics have shown that compressive and shear strength of a polycrystalline armor ceramic do not seem to deteriorate under single shock (Dandekar and Benfanti 1993) and release or under repeated shock-release loading cycle (Dandekar 1994a, 1994b). On the other hand, tensile strengths (i.e., spall threshold) degrade significantly both when subjected to increasing magnitude of impact stress under single shock and release and under repeated shock-release cycle (Dandekar 1992, Dandekar and Benfanti 1993; Dandekar and Bartkowski 1994). Additionally, it has been suggested that the presence of minor void-volume fraction and microcracks in ceramics do not

degrade their compressive properties significantly (Ewart and Dandekar 1994). The tensile strengths of these materials, however, are very sensitive to the presence of voids and microcracks. Briefly, as long as a ceramic is under compression under uniaxial strain condition, these flaws do not significantly reduce its compressibility or shear strength, but, as soon as a flawed material is subjected to tensile loading condition, propagation of microcracks degrade tensile strength of the material significantly.

The present work was initiated to measure and compare tensile strengths (i.e., spall thresholds) of five different types/varieties of silicon carbide (SiC) materials. Three types of SiC were manufactured in the United States. The remaining two varieties of SiC were manufactured in France. Spall strengths of these five different SiC materials were measured by performing plane shock wave experiments to a maximum impact-generated stress level of 17 GPa on the light gas-gun facility at the U.S. Army Research Laboratory (ARL). It is planned to recover shock-deformed material in future experiments to determine the statistics of microcracks in order to investigate their role in the observed spall strength. The results of the present work also offer new challenges to modeling ceramic materials since the tensile strength (measured spall strengths) of SiC initially increases with an increase in the impact stress before showing a decline at higher impact stresses.

## **2. Materials**

**2.1 U.S. Materials.** SiC materials were produced either by sintering or by hot-pressing SiC powder. The sintered SiC was manufactured by Sohio, and the remaining two hot-pressed materials, SiC-B and SiC-N, were manufactured by Cercom, Inc. The processing of SiC being proprietary, the details of processing are not disclosed by the manufacturers. Mechanical properties of SiC produced by either of the aforementioned two means are dependent on grain size of the powder, processing temperature, sintering aids, powder-blending process, and elemental composition and stoichiometry of the compounds present in the processed materials. All powders have some metallic impurities. These are introduced during the powder

manufacturing process. In addition, SiC cannot be consolidated without sintering aids. The conventional sintering aids for consolidating SiC powder are boron, carbon, and aluminum nitride.

**2.1.1 Sohio Material: Sintered SiC.** The Sohio sintered material is produced from SiC powder mixed with sintering aids. The mixed powder is precompacted to roughly 70% of the theoretical density of fully compacted SiC or single-crystal density. The precompact material is then heated to 2,023–2,473 K for sintering. Since sintered material uses thermal energy for densification, the resultant material never achieves the theoretical density and has a porosity in the range of 2–5%. The grain size varied between 2 and 15  $\mu\text{m}$ , with an average grain size of 4  $\mu\text{m}$ .

**2.1.2 Hot-Pressed SiC SiC-B.** SiC-B material uses aluminum nitride as an sintering aid. This material has a unique microstructure. All impurities segregate in small, well-dispersed clusters along the SiC grain boundaries. The blended powder, containing SiC and sintering aid, is loaded into a graphite die and then hot-pressed at around 2,273 K under 18 MPa. Since 2,273 K is higher than the melting temperature of the metallic impurities, the melted metals can aggregate to form inclusions in the consolidated SiC. Sintering aids promote formation of these inclusions through creating favorable environs to wet SiC grain, surfaces, thus spreading the melt. The average grain size of this material is 4  $\mu\text{m}$  with the size ranging between 2–10  $\mu\text{m}$ .

**2.1.3 Hot-Pressed SiC SiC-N.** SiC-N is a refined product of SiC-B, with a proprietary powder homogenization and use of organic binder. The organic binder burns out during the hot-pressing of the powder, leaving behind some carbon, which depletes the oxide layer on the powder. The net effect is to reduce the glassy oxide phase in the final consolidated product. The average grain size of SiC-N is 4  $\mu\text{m}$ . The range of grain sizes lies between 1–8  $\mu\text{m}$ . Shih (1998) provides additional details about the manufacturing of these two Cercom SiC.

**2.2 French SiC.** Ceramiques & Composites Society manufactured sintered French material by the pressureless sintering process. The pore volume fraction in the material is 4.2%. The mean pore size is 1–2  $\mu\text{m}$ . SiC grains are equiaxed with a mean grain diameter being 6  $\mu\text{m}$ . Sintering was facilitated by the addition of carbon and boron, which led to formation of boron carbide in the material. The mean size of boron carbide particles are  $3.0 \pm 1.8 \mu\text{m}$ . Free carbon particles are also present in the materials.

Sintered material, described previously, was hot-pressed to obtain French sintered and hot-pressed SiC. The hot processing reduced the pore volume fraction in the hot-pressed material to 2.5%. The mean grain size, the composition, and the crystallographic configuration remained the same as in the sintered material.

### **3. Material Properties**

The following properties were determined/investigated before shock wave experiments were performed: elemental composition, average grain size and microstructure, density, and elastic constants.

**3.1 Elemental Composition.** The elemental compositions of the five Sic materials (in weight percentage) are given in Table 1. These five materials have comparable impurities contained in them. These minor differences themselves may possibly influence the tensile strength of these materials only through the presence of glassy phase and pore volume fraction in the materials serving as the weak links in the cohesivity of the materials.

**3.2 Microstructure.** Micrographs showing the grain structure of each of the five materials are given in Figures 1–5. Micrographs were taken at 1,000 $\times$ . These figures display no significant difference in the microstructures of these materials at the magnification shown, except that the sintered materials have larger porosity than the hot-pressed materials. The Sohio and French sintered and hot-pressed materials showed evidence of elongated grain growth in their

**Table 1. Elemental Compositions of SiC Materials (in Weight Percentage)**

Element	Atomic Mass	Sohio	Cercom SiC-B	Cercom SiC-N	French SiC
Si	28.09	68.51	69.50	69.25	68.40
C	12.01	29.66	29.82	29.31	30.60
Al	26.98	0.03	<0.01	1.00	0.035
N	14.01	0.026	0.176	—	0.37
Fe	55.85	0.02	0.30	0.10	0.03
O	16.00	0.023	0.113	—	0.30
S	32.06	0.024	0.027	—	0.026
Ti	47.90	0.01	—	0.04	0.013
Zr	91.22	0.02	<0.01	0.03	—
V	50.94	—	0.02	0.02	—
Mg	24.31	<0.01	0.02	—	0.015
Ni	58.71	—	—	0.03	—
Ca	40.08	0.02	—	<0.01	—
Co	58.93	—	0.02	—	—
Cr	52.00	—	—	0.01	0.006
Cu	63.54	—	0.01	—	0.003
Na	22.99	0.01	—	—	—
Hf	178.49	—	0.01	—	—
P	30.97	—	0.01	—	—
B	10.81	—	<0.01	—	—
W	183.85	—	—	—	<0.01

micrographs. These micrographs do not indicate a significant population of cracks or microcracks.

**3.3 Density and Elastic Constants.** The densities of five materials were measured by Archimedes method. Their elastic constants were obtained from the measured ultrasonic longitudinal and shear wave velocities. The wave velocities were measured by wave overlap technique (Papadakis 1967). The ultrasonic longitudinal and shear wave velocities were performed at 10 and 5 MHz, respectively. The average values of density and wave velocities are given in Table 2.

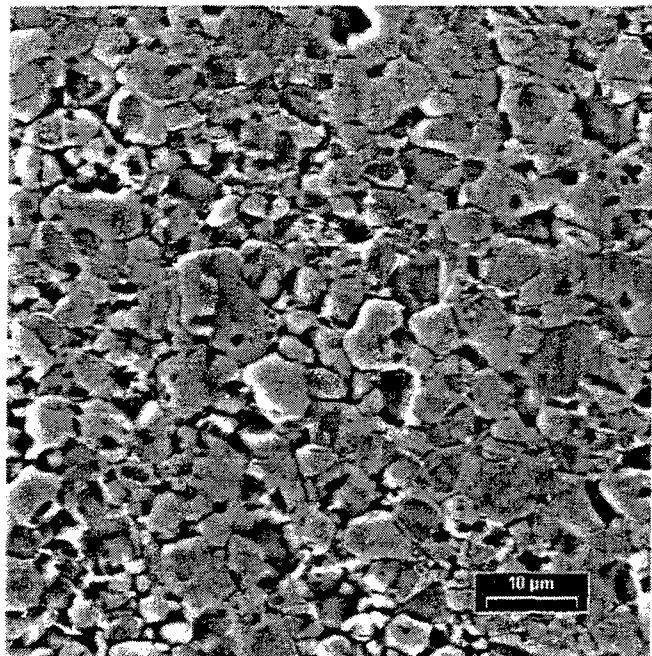


**Figure 1. Microphotograph of Sohio Sintered SiC.**

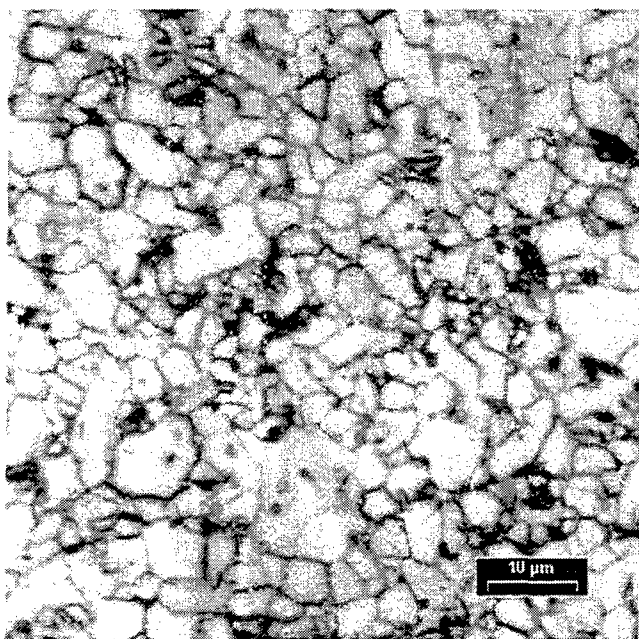


**Figure 2. Microphotograph of French Sintered SiC.**

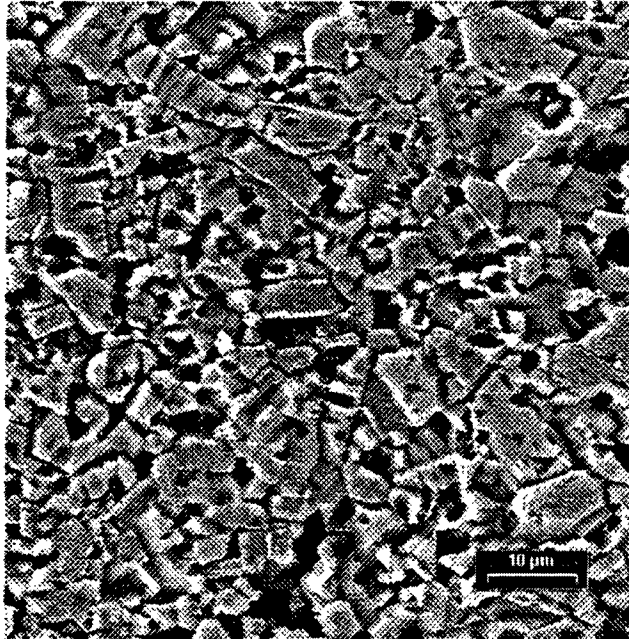


**Figure 3. Microphotograph of Hot-Pressed SiC-B.**

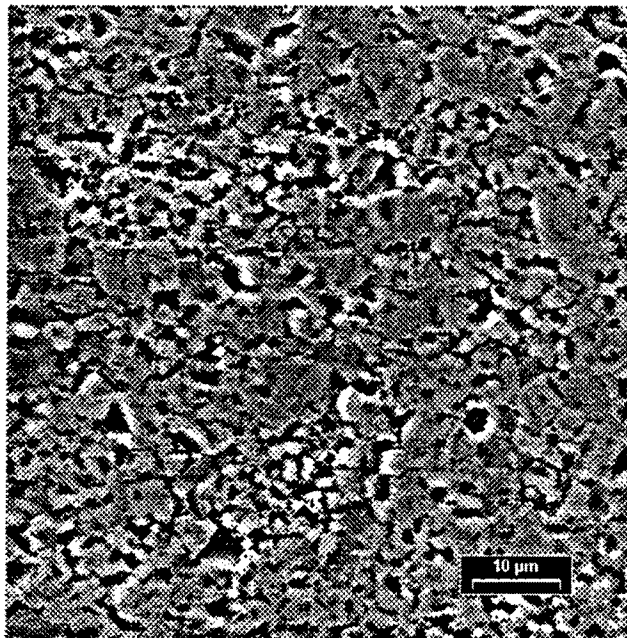


**Figure 4. Microphotograph of Hot-Pressed SiC-N.**

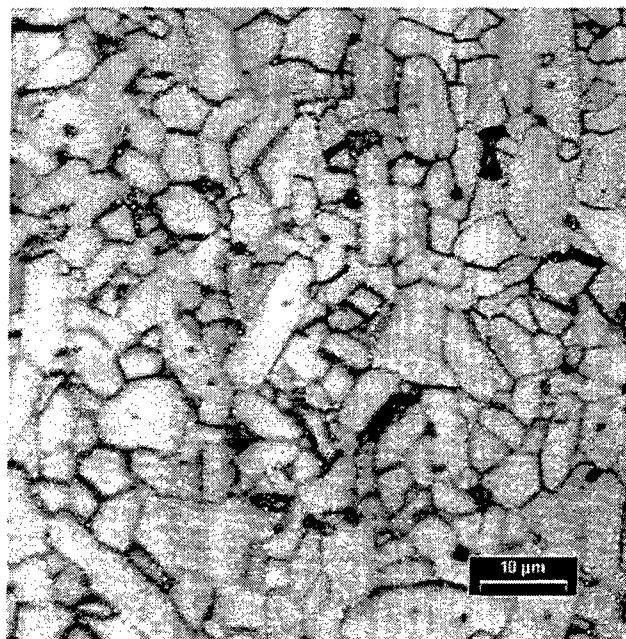


**Figure 5. Microphotograph of French Sintered and Hot-Pressed SiC.**

**Table 2. Density and Ultrasonic Wave Velocities of Five SiC Materials**

Property	Sintered		Hot-Pressed		
	Sohio	French	French	SiC-B	SiC-N
No. of Samples	4	5	5	8	6
Density (Mg/m <sup>3</sup> )	3.164 ± 0.004	3.137 ± 0.001	3.184 ± 0.003	3.215 ± 0.002	3.227 ± 0.001
Wave Velocity, Longitudinal (km/s)	12.044 ± 0.015	12.055 ± 0.003	12.186 ± 0.007	12.198 ± 0.026	12.262 ± 0.001
Shear	7.664 ± 0.011	7.670 ± 0.007	7.730 ± 0.010	7.747 ± 0.018	7.774 ± 0.005

**3.3.1 Density.** SiC has either cubic ( $\beta$ ) or hexagonal crystal ( $\alpha$ ) structures but has numerous polytypes. The densities of  $\beta$ -SiC and  $\alpha$ -SiC are 3.216 and 3.219 Mg/m<sup>3</sup>, respectively. Solid-state sintering at and above 2,273 K leads to transformation of  $\beta$ -SiC to  $\alpha$ -SiC. Hence, the density of SiC produced under the aforementioned condition is expected to be 3.219 Mg/m<sup>3</sup>. Further, SiC-B and SiC-N are 6H polytype materials. The density of  $\alpha$ -SiC (6H) is 3.215 Mg/m<sup>3</sup>. Consideration of the aforementioned facts regarding the expected variation in

the density of SiC implies that the sintered SiC made by Sohio has relatively less void volume than the French sintered material.

Belayt and Cottenot (1996) reported that French SiC material is primarily in 6H polytype phase though 4H polytype is also found to be present. They report density values of the French sintered and sintered and hot-pressed materials to be 3.13 and 3.17 Mg/m<sup>3</sup>. Table 2 shows that these are in good agreement with this report's measurements of densities of these materials. The densities of SiC-B and SiC-N indicate them to be fully dense, but the French sintered and HIP material appears to have estimated porosity measured by void-volume fraction to be 3.7%.

**3.3.2 Elastic Constants.** The measured values of ultrasonic wave velocities as a function of density of these materials are shown in Figure 6. The longitudinal wave velocities vary between 12.04 and 12.26 km/s. The shear wave velocities vary between 7.66 and 7.77 km/s. The variation of the wave velocities with density is linear. Belayt and Cottenot (1996) reported the longitudinal and shear wave velocities for the sintered material as 11.8 and 7.6 km/s, respectively. The measurement of the longitudinal wave velocity reported here is reported here slightly higher than their measurement, but the differences are in all probability not significant. Shear wave velocity measurements are in very good agreement with one another. They also report the values of the longitudinal and shear wave velocities for the sintered and hot-pressed SiC to be 12.1 and 7.7 km/s, respectively. These values agree with the measurements given in Table 2. A detailed analysis of this variation of velocity with density using an existing model dealing with the variation of elastic properties of materials with porosity is under preparation.

The values of elastic constants of SiCs calculated from the measured densities and ultrasonic wave velocities are presented in Table 3. This table shows that the values of elastic constants of sintered materials are relatively smaller in magnitude than those of hot-pressed materials, but these values are within the precision of these measurements for each type. In other words, the elastic constants of three hot-pressed and two sintered materials do not differ from one another significantly for similarly produced materials. Poisson's ratios of the five materials appear to be process independent and vary between 0.160 and 0.164.

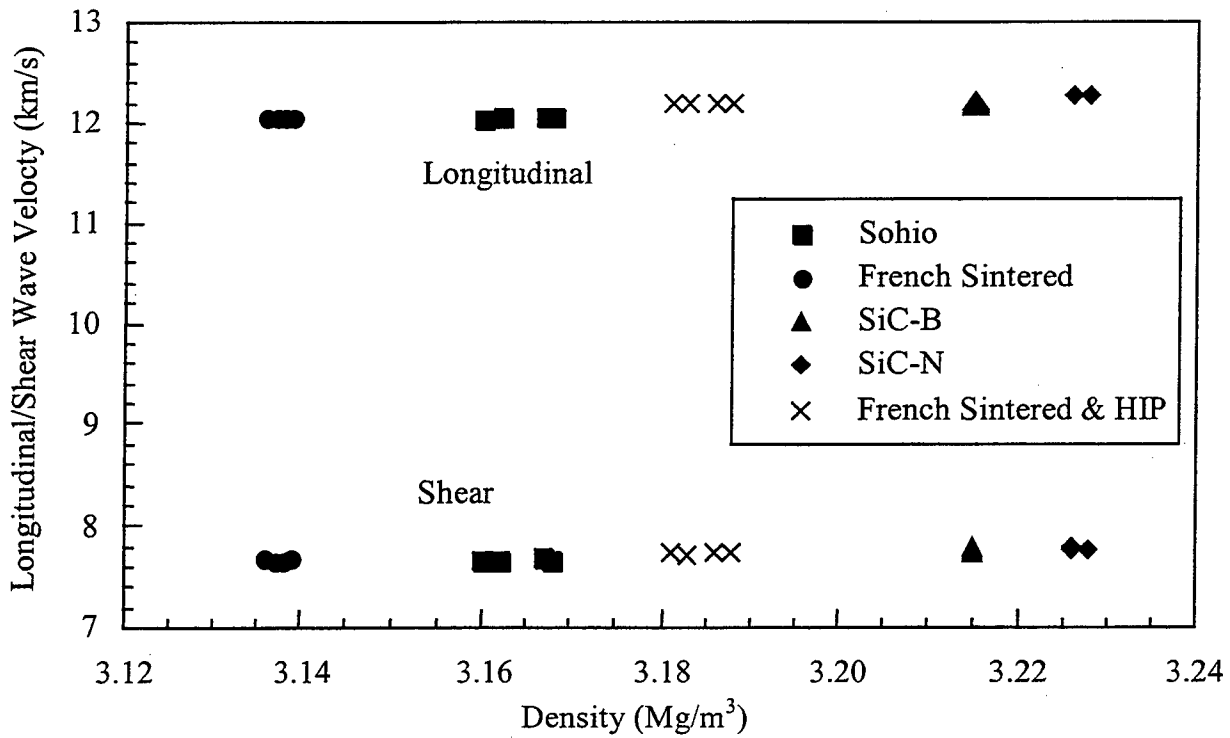


Figure 6. Variation in Ultrasonic Wave Velocities as a Function of Density in SiC.

Table 3. Elastic Constants of SiC Materials

Property	Sintered		Hot Pressed		
	Sohio	French	French	SiC-B	SiC-N
Density (Mg/m <sup>3</sup> )	3.164 ± 0.004	3.137 ± 0.001	3.184 ± 0.003	3.215 ± 0.002	3.227 ± 0.001
Modulus (GPa)					
Shear	185.8 ± 0.7	184.6 ± 0.3	190.3 ± 0.4	193.0 ± 0.9	195.0 ± 0.2
Bulk	211.2 ± 0.6	209.8 ± 0.5	219.1 ± 1.0	221.1 ± 1.8	225.2 ± 0.3
Young	431.2 ± 0.9	428.1 ± 0.9	442.5 ± 1.3	448.4 ± 2.1	454.0 ± 0.6
Poisson's Ratio	0.160 ± 0.001	0.160 ± 0.001	0.163 ± 0.002	0.162 ± 0.003	0.164 ± 0.001

## 4. Design of Shock Experiments

Two configurations used to perform spall experiments on SiC are shown in Figure 7. The experiment consists of impacting a stationary plate of SiC with a thinner plate of one of the following: SiC, z-cut sapphire, or tungsten carbide (WC) at a given impact velocity. In one case, the particle velocity profile is recorded at the stationary plate poly-methyl-meth-acrylate (PMMA) window interface (Figure 7a). In the second case, the free-surface velocity profile of the stationary plate is monitored (Figure 7b). The wave velocity profiles were recorded by means of a 4-beam velocity interferometer system for any reflector (VISAR) (Barker and Hollenbach 1972). In symmetric impact configuration (Figure 7), the impactor disk was generally half the thickness of the target disk, creating a spall plane in the center of the target disk. The flyers and targets were  $3.949 \pm 0.077$  mm and  $7.944 \pm 0.098$  mm in thickness, respectively, yielding a pulse width of  $0.641 \pm 0.033$   $\mu$ s. A few experiments were done where the impactors were either z-cut sapphire or WC. In these cases, the pulse width deviated from those in symmetric experiments on SiC. These experiments have been identified in the relevant tables, where the summary of shock wave experiments on various SiC are presented. All specimens were  $39.5 \pm 0.5$  mm in diameter. SiC disk faces were lapped and polished flat to 5  $\mu$ m, while the opposing disc faces were mutually parallel to within one part in  $10^4$ .

The stress-particle velocity diagram for the aforementioned experiment is shown in Figure 8. The figure depicts deformation of an elastic-inelastic material. Upon impact, stress-particle velocity coordinates defining the shock state of the material are  $(\sigma_1, u_1)$  in Figure 8. For the configuration Figure 7a, the measured particle velocities correspond to  $\sigma_3$ ,  $\sigma_4$ , and  $\sigma_5$  on the PMMA Hugoniot in Figure 8. These correspond to initial compression, release from the initial compressed state, and reshock from the release state of the window material (i.e., PMMA). In addition, the data analysis for this configuration is carried out assuming that the shock, release, and reshock response of PMMA can be represented by its initial shock response and its properties are time independent. The Hugoniot determined by Barker and Hollenbach (1972) is used. It should be noted that, for a linear elastic material, the points  $u_3$  and  $u_5$  will be coincident.

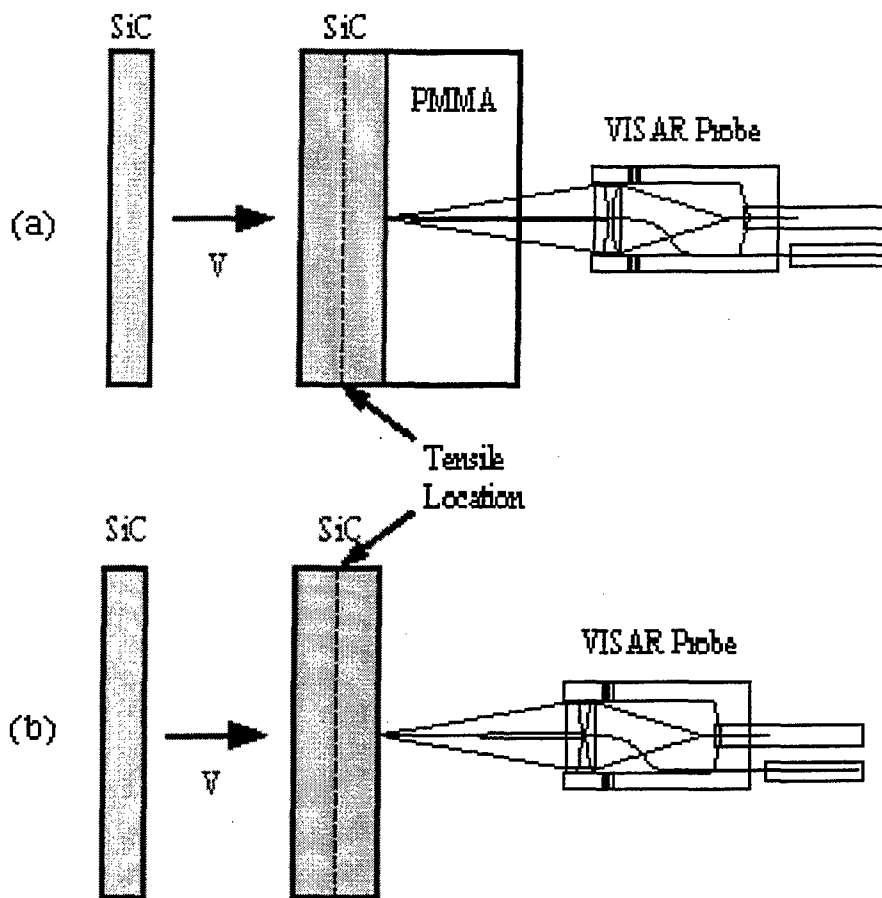


**Figure 7. Two Configurations of Symmetric Transmission Experiments (a) With a PMMA Window and (b) Without a PMMA Window.**

For the configuration Figure 7b, free-surface velocities measured correspond to  $u_2$ ,  $u_8$ , and  $u_9$ . Further, as in the previous case, free-surface velocities corresponding to  $u_2$  and  $u_9$  are the same for a linear elastic material.

When PMMA was used as a window material in an experiment, aluminum was vapor-deposited at the SiC-PMMA interface to enhance reflectivity for the VISAR beam. In the absence of a PMMA window, a SiC specimen surface was polished to reflect the VISAR beam. The flyer disk impact velocity was varied to produce impact stresses between 1.57 and 16 GPa.



and after spallation to calculate spall stress. Shock and tensile paths during the impact event are schematically shown in the stress vs. particle velocity plot of Figure 8. The spall threshold is calculated using the peak steady particle velocity recorded before spallation and the pull-back signal from spallation. For the experiment configuration (Figure 7a), the spall strength ( $\sigma_T', u_T'$ ) is calculated by the intersection of states ( $\sigma_3, u_3$ ) and ( $\sigma_4, u_4$ ) using the elastic impedance of the SiC. Using the buffered VISAR configuration offers a second method of calculating the spall strength. The spall strength can also be calculated from the intersection of lines from ( $0, u_5'$ ) and ( $\sigma_4, u_4$ ), where ( $0, u_5'$ ) is determined from the recorded state ( $\sigma_5, u_5$ ) using the elastic impedance for SiC. Under linearly elastic response, the intersection of lines from steady states before ( $\sigma_3, u_3$ ) and after spall ( $\sigma_5, u_5$ ) with the particle velocity axis will be identical with coordinate ( $0, u_5'$ ). The linear assumption is valid for a linearly elastic material. In other words, any difference in the calculated values of spall stress by these two methods provides some indication that the material is not linearly elastic. The other implicit assumption is that initial shock response of PMMA is representative of its release and reshock response. Recent studies by Dandekar and coworkers (Dandekar et al. 1988; Bartkowski and Dandekar 1997, 1999) throw doubts on the validity of latter assumption about the shock response of PMMA when impact induced stress exceeds its Hugoniot elastic limit (HEL) (i.e., 0.7 GPa).

For the configuration shown in Figure 7b, the spall state ( $\sigma_T, u_T$ ) is determined by the intersection of lines from the peak steady state ( $0, u_2$ ) and pull-back state ( $0, u_8$ ) using SiC elastic impedance. Similar to the previous case,  $u_2$  and  $u_8$  are equal in magnitude for a linear elastic material. Representative wave profiles recorded for these five SiC materials in experiments performed at impact velocities of 0.08 and 0.6 km/s are shown in Figures 9 and 10. The wave profile for Sohio material at 0.6 km/s was recorded at PMMA-SiC interface. Hence, the magnitude of particle velocity related to impact-induced shock is less than the magnitude of impact velocity. These wave profiles show no clear-cut evidence of inelastic deformation in these five SiC. Further, the magnitude of free-surface velocity due to release of shock and recompression following the spallation in these material do not differ significantly or systematically with the impact velocity for these materials (Tables 4–8), indicating an elastic

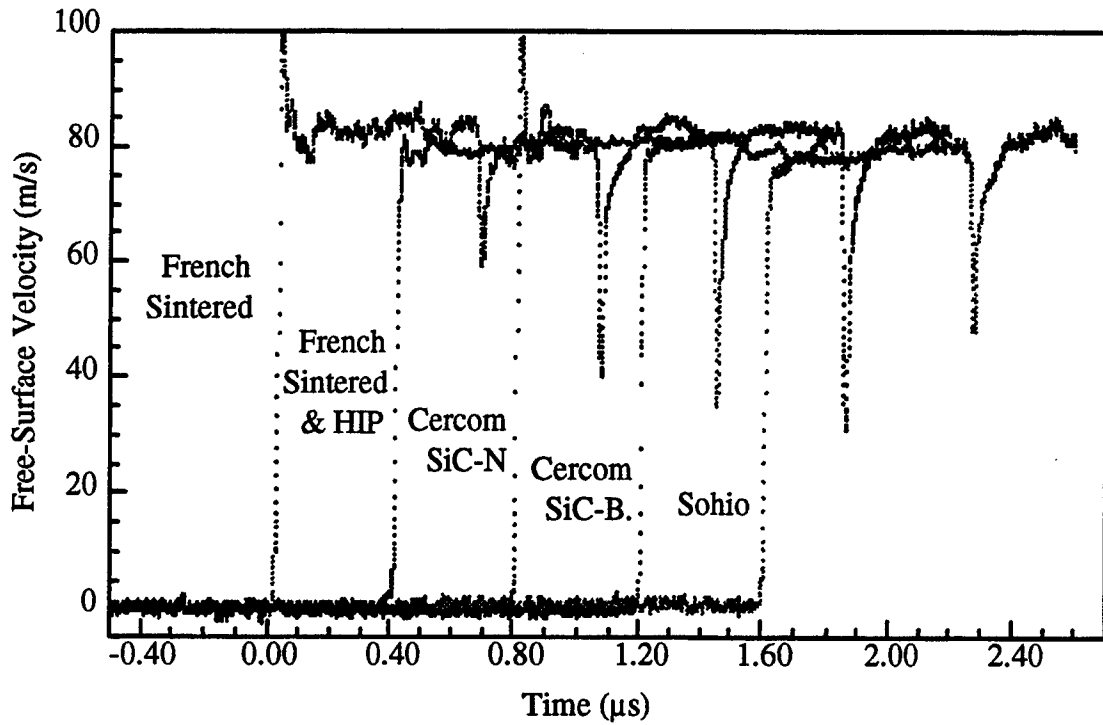


Figure 9. Free-Surface Velocity in Profiles in SiC, Impact Velocity 0.08 km/s.

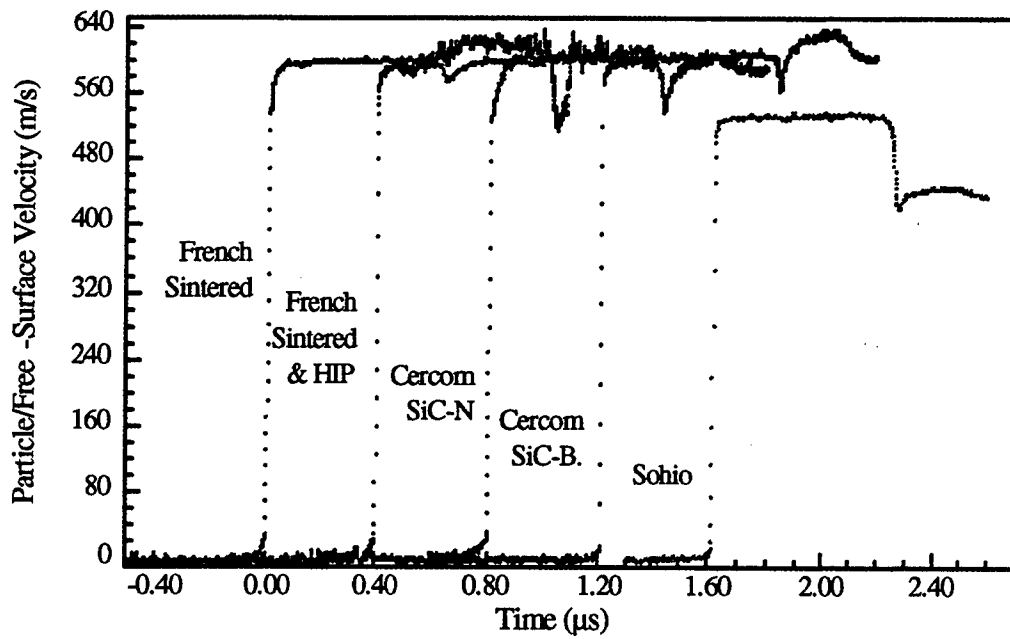


Figure 10. Velocity Profiles in SiC, Impact Velocity 0.6 km/s.

**Table 4. Data From Transmission Experiments on Sohio Sintered SiC**

Experiment	Thickness (mm)		Impact Velocity (km/s)	Pulse Width ( $\mu$ s)	Free-Surface/Particle Velocity (km/s)		
	Flyer	Target			Shock	Spall	Recompression
404 <sup>a</sup>	3.948	8.012	0.6021	0.636	0.5351	0.4212	0.4449
413 <sup>a</sup>	3.965	8.002	0.0826	0.662	0.0760	0.0353	0.0630
421 <sup>a</sup>	3.997	7.966	0.2939	0.650	0.2673	0.1892	0.2180
423	4.018	7.951	0.1907	0.657	0.1922	0.1414	0.1900
433 <sup>a</sup>	4.009	7.950	0.0804	0.671	0.0733	0.0261	0.0635
441	3.993	7.973	0.4523	0.650	0.4575	0.4307	0.4600
443	3.944	7.770	0.1483	0.653	0.1535	0.1180	0.1524
447	3.932	7.964	0.4956	0.640	0.5093	0.4730	0.5044
452	3.981	7.977	0.0804	0.659	0.0806	0.0480	0.0820

<sup>a</sup> In this experiment, a 6-mm-thick PMMA disk was bonded to the SiC target and particle velocity profile was monitored at the PMMA-SiC interface.

**Table 5. Summary of the Results of Transmission Experiments on Sohio Sintered SiC**

Experiment	Impact Velocity (km/s)	Shock State		Release Impedance ( $Gg/m^2 \cdot s$ )	Spall Strength			
		Mass Velocity (km/s)	Stress (GPa)		1/2 Pull-Back Change (km/s)	Stress (1) (GPa)	Stress (2) (GPa)	
404 <sup>a</sup>	0.6021	0.3011	11.484	39.81	—	—	0.271	0.503
413 <sup>a</sup>	0.0826	0.0413	1.575	37.60	—	—	0.578	0.578
421 <sup>a</sup>	0.2939	0.1470	5.606	38.28	—	—	0.638	0.602
423	0.1907	0.0954	3.637	37.55	0.0254	—	0.967	0.925
433 <sup>a</sup>	0.0804	0.0402	1.533	38.45	—	—	0.723	0.779
441	0.4523	0.2262	8.627	37.29	0.0134	—	0.511	0.558
443	0.1483	0.0742	2.829	35.65	0.0178	—	0.678	0.655
447	0.4956	0.2478	9.453	36.15	0.0182	—	0.693	0.598
452	0.0804	0.0402	1.533	37.96	0.0163	—	0.621	0.648

<sup>a</sup> In this experiment, a 6-mm-thick PMMA disk was bonded to the SiC target and particle velocity profile was monitored at the PMMA-SiC interface.

**Table 6. Data From Transmission Experiments on French Sintered SiC**

Experiment	Thickness (mm)		Impact Velocity (km/s)	Pulse Width ( $\mu$ s)	Free-Surface Velocity (km/s)		
	Flyer	Target			Shock	Spall	Recompression
528	3.973	8.014	0.6098	0.659	0.5993	0.5736	0.5993
530	3.969	8.003	0.1853	0.658	0.1804	0.1472	0.1743
531	3.953	7.998	0.0808	0.656	0.0846	0.0593	0.0800
802 (WC)	2.008	6.016	0.527	0.570	0.7644	0.7505	0.762
807	2.034	6.016	0.5934	0.337	0.5951	0.5788	0.5921
812	4.006	6.015	0.384	0.665	0.3774	0.3585	0.3756
824-1	4.023	6.014	0.3042	0.667	0.3044	0.2709	0.3024

**Table 7. Summary of the Results of Transmission Experiments on French Sintered SiC**

Experiment	Impact Velocity (km/s)	Shock		Release Impedance ( $Gg/m^2 \cdot s$ )	Spall Strength	
		Mass Velocity (km/s)	Stress (GPa)		1/2 Pull-Back Change (km/s)	Stress (GPa)
528	0.6098	0.3049	11.531	39.17	0.0129	0.488
530	0.1853	0.0927	3.504	39.93	0.0166	0.628
531	0.0808	0.0404	1.528	34.57	0.0127	0.480
802 (WC)	0.527	0.3917	14.814	39.75	0.0070	0.265
807	0.5934	0.2967	11.221	37.60	0.0081	0.306
812	0.384	0.1920	7.261	39.17	0.0095	0.359
824-1	0.3042	0.1521	5.752	37.77	0.0168	0.635

Table 8. Data From Transmission Experiments on SiC-B

Experiment	Thickness (mm)		Impact Velocity (km/s)	Pulse Width ( $\mu$ s)	Free-Surface Velocity (km/s)		
	Flyer	Target			Shock	Spall	Recompression
404 <sup>a</sup>	3.890	7.950	0.6021	0.613	0.5383	0.4015	0.4272
413 <sup>a</sup>	3.914	7.935	0.0826	0.630	0.0752	0.0243	0.0585
421 <sup>a</sup>	3.915	7.926	0.2939	0.632	0.2725	0.1730	0.2270
423	3.934	7.957	0.1907	0.623	0.1923	0.1263	0.1925
433 <sup>a</sup>	3.920	7.901	0.0804	0.628	0.0654	0.0125	0.0571
437	3.910	7.951	0.1330	0.636	0.1316	0.0859	0.1312
443	3.912	7.967	0.1483	0.643	0.1535	0.1073	0.1540
447	3.905	7.932	0.4956	0.613	0.5093	0.4593	0.5093
452	3.974	7.918	0.0804	0.642	0.0823	0.0307	0.0832
504	3.984	7.916	0.6130	0.633	0.6059	0.5615	0.6056
607	2.122	7.958	0.1311	0.334	0.1305	0.0872	0.1326

<sup>a</sup> In this experiment, a 6-mm-thick PMMA disk was bonded to the SiC target and particle velocity profile was monitored at the PMMA-SiC interface.

response. Dandekar (1996) measured the tensile impedance of SiC-B to be  $40.0 \pm 1.1 \text{ Gg/m}^2\cdot\text{s}$ . The value of its elastic impedance from the ultrasonic longitudinal wave velocity measurement and density is  $39.2 \pm 0.1 \text{ Gg/m}^2\cdot\text{s}$ . In view of the aforementioned, the spall threshold values for these materials are calculated using their respective elastic impedances.

**5.2 Results of Spall Experiments.** Results of spall experiments are described by grouping the materials according to the manufacturing process rather than the country of origin.

**5.2.1 Sintered SiC.** The results of shock wave experiments performed on sintered SiC manufactured in the United States and France are summarized as follows. Tables 4 and 6 give the data collected for shock wave experiments conducted on sintered SiC. Tables 5 and 7 give the values of impact stress, associated particle velocity, release impedance calculated from impact stress, measured particle velocity and release particle velocity, half the pull-back change in the particle velocity, and spall strength of sintered SiC. Impact stresses were calculated by multiplying the longitudinal impedance of a material by the appropriate value of the particle velocity. In case of symmetric experiments, it was simply half the magnitude of the impact velocity. In other cases, it was determined from the known Hugoniot of the impactor and assumed elastic deformation of SiC. This is a reasonable procedure because the free-surface velocity profiles do not show compelling evidence of inelastic or irreversible deformation suffered by SiC in the range of impact stress generated in these experiments.

The data for Sohio sintered SiC shows that it deforms elastically when shocked to 11.5 GPa. The evidence for this comes from the measured pulse widths (Table 4) and values of release impedance, varying between 36 and 40  $\text{Gg/m}^2\cdot\text{s}$  (the elastic impedance being 38  $\text{Gg/m}^2\cdot\text{s}$ ), and free-surface velocity being equal to the impact velocity (Table 5). The discrepancy in the values of spall strength calculated from measured values of  $(\sigma_3, u_3)$  and  $(\sigma_4, u_4)$ , and  $(\sigma_5, u_5)$  and  $(\sigma_4, u_4)$  for experiment 404 may arise from the assumption that the response of PMMA under initial shock, also represents its response under subsequent release and reshock, and possibly the reshock following the spall is not elastic. All other pairs of

calculated spall strength values agree with one another. Figure 11 shows the variation in the values of the spall strength of Sohio SiC with impact stress. It is clear from the figure that the variability in the spall strengths of Sohio sintered SiC with impact stress exceeds the precision of measurements, thereby suggesting that, even though its response under shock compression and release is elastic within the precision of these reported measurements, its tensile strength is influenced by material variability. The material variability may be either due to processing variation from batch to batch or difference in the evolution of microcracks and/or other defects. Additionally, a clear trend for a gradual decline in its spall strength with an increase in impact stress is evident from Figure 11. Experiments were not able to be performed in this material at higher stresses to determine the impact stress at and beyond which it has no spall strength.

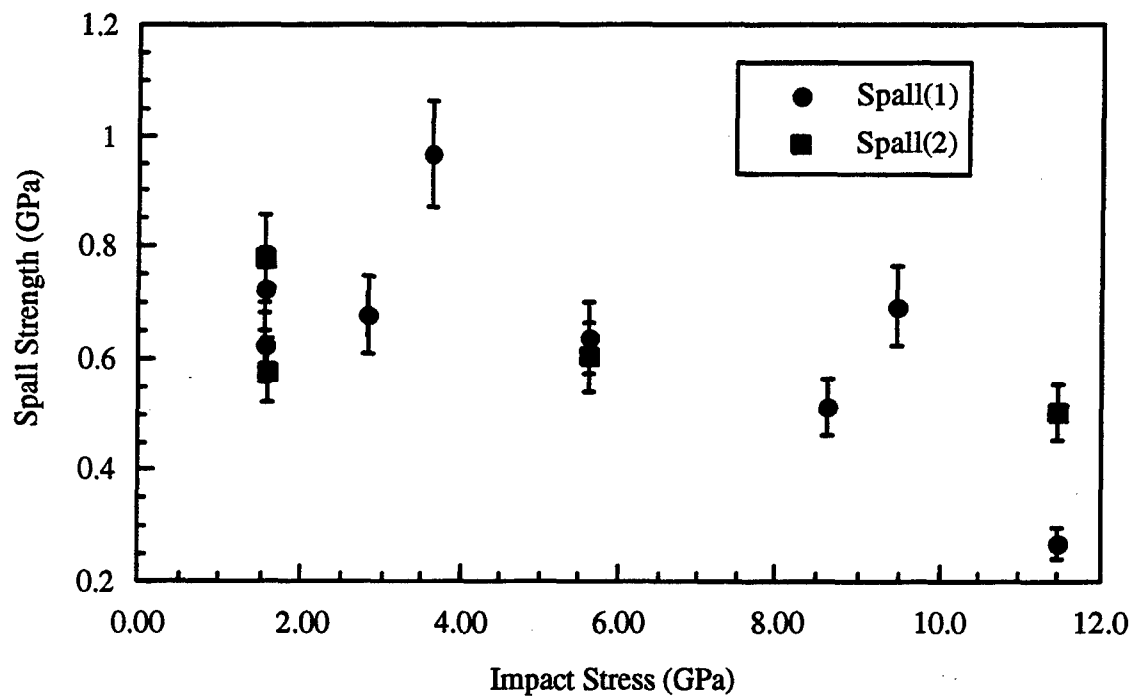


**Figure 11. Spall Strength vs. Impact Stress of Sohio SiC.**

The general characteristics of the deformation of French sintered SiC under shock compression (Figure 12) is similar to that of Sohio sintered SiC. However, two observations pertaining to this material are worth pointing out: (1) the magnitude of spall strength at each

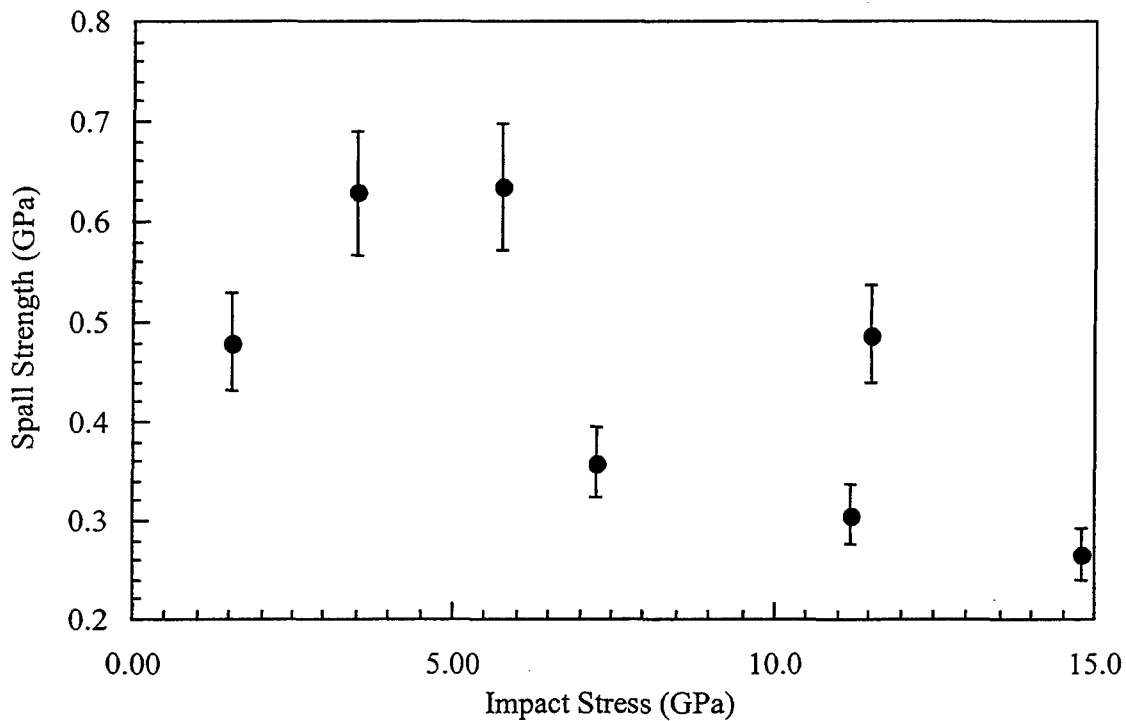


**Figure 12. Spall Strength vs. Impact Stress of French Sintered SiC.**

comparable stress is smaller than the corresponding values of spall strength of Sohio SiC and (2) two experiments conducted at impact stress of 11.2 and 11.5 GPa show that reduction of pulse width actually lowers its spall strength. It is difficult to explain such a behavior unless the specimens used in these experiments had drastically different population of microdefects.

**5.2.2 Hot-Pressed SiC.** The results of shock wave experiments on SiC-B and SiC-N are summarized in Tables 8–11. As mentioned earlier, SiC-N is a refined product of SiC-B, with a proprietary powder homogenization and use of organic binder. The organic binder burns out during the hot-pressing of the powder, leaving behind some carbon, which depletes the oxide layer on the powder. The net effect is to reduce the glassy oxide phase in the final consolidated product. Thus, it is expected that difference in the spall behavior of these two hot-pressed materials will be partly due to lesser amount of glassy phase in SiC-N compared to in SiC-B. An implicit assumption in this statement is that batch-to-batch variations in these two SiC materials are insignificant and do not affect the shock response significantly.

**Table 9. Summary of The Results of Transmission Experiments on SiC-B**

Experiment	Impact Velocity (km/s)	Shock		Release Impedance (Gg/m <sup>2</sup> s)	1/2 Pull-Back Change (km/s)	Spall Strength	
		Mass Velocity (km/s)	Stress (GPa)			Stress (1) (GPa)	Stress (2) (GPa)
404 <sup>a</sup>	0.6021	0.3011	11.845	40.73	—	0.822	0.560
413 <sup>a</sup>	0.0826	0.0413	1.625	40.04	—	0.823	0.732
421 <sup>a</sup>	0.2939	0.1470	5.782	37.93	—	1.123	1.160
423	0.1907	0.0954	3.752	38.70	0.0330	1.294	1.299
433 <sup>a</sup>	0.0804	0.0402	1.582	53.56	—	0.903	0.955
437	0.1330	0.0665	2.617	40.19	0.0228	0.894	0.890
443	0.1483	0.0742	2.918	36.77	0.0231	0.906	0.917
447	0.4956	0.2478	9.750	37.28	0.0250	0.980	0.982
452	0.0804	0.0402	1.582	37.57	0.0258	1.012	1.025
504	0.6130	0.3056	12.06	40.28	0.0222	0.871	—
607	0.1311	0.0656	2.57	39.6	0.0216	0.847	—

<sup>a</sup>In this experiment, a 6-mm-thick PMMA disk was bonded to the SiC target and particle velocity profile was monitored at the PMMA-SiC interface.

Table 10. Data From Transmission Experiments on SiC-N

Experiment	Thickness (mm)		Impact Velocity (km/s)	Pulse Width ( $\mu$ s)	Free-Surface Velocity (km/s)		
	Flyer	Target			Shock	Spall	Recompression
519	3.987	8.009	0.1683	0.650	0.1748	0.1474	0.1711
520	3.985	7.992	0.6049	0.650	0.6062	0.5389	0.5895-0.6000
522	3.962	7.975	0.0809	0.646	0.0809	0.0352	0.0807
525	3.983	7.994	0.4014	0.650	0.3973	0.3638	0.3947
528	3.958	55.99	0.6098	0.646	0.6049	0.5383	0.6019
607	3.986	5.937	0.1311	0.713	0.1463	0.0931	0.1451
617 (Sapphire)	3.996	5.016	0.2903	0.715	0.3031	0.2681	0.3031
621	4.001	7.354	0.3912	0.653	0.4211	0.3533	0.4204
628	3.961	5.989	0.2889	0.646	0.2885	0.2478	0.2885-0.2854
636 (SiC-B)	2.108	4.008	0.1499	0.346	0.1498	0.1026	0.1509
824-2	4.022	5.983	0.3042	0.656	0.3069	0.2598	0.3071

**Table 11. Summary of the Results of Transmission Experiments on SiC-N**

Experiment	Impact Velocity (km/s)	Shock		Release Impedance (Gg/m <sup>2</sup> ·s)	Spall Strength	
		Mass Velocity (km/s)	Stress (GPa)		1/2 Pull-Back Change (km/s)	Stress (GPa)
519	0.1683	0.0842	3.330	36.73	0.0137	0.542
520	0.6049	0.3025	11.968	39.40	0.0337	1.334
522	0.0809	0.0405	1.601	39.57	0.0229	0.906
525	0.4014	0.2007	7.942	40.40	0.0168	0.665
528	0.6098	0.3049	12.065	40.22	0.0333	1.318
607 (Sapphire)	0.1311	0.0694	2.746	35.70	0.0266	1.052
617 (Sapphire)	0.2903	0.1537	6.080	30.78	0.0175	0.692
621	0.3912	0.1956	7.740	34.32	0.0339	1.341
628	0.2889	0.1445	5.716	39.68	0.0204	0.807
636 (SiC-B)	0.1499	0.0746	2.953	39.27	0.0236	0.934
824-2	0.3042	0.1521	6.019	38.88	0.0236	0.934

5.2.2.1 *SiC-B*. The pulse widths in all the experiments except experiment 607, were 0.61–0.64  $\mu\text{s}$ . The pulse width in experiment 607 was 0.33  $\mu\text{s}$ . Its spall strength also shows a trend similar to the one showed by sintered SiC previously mentioned. The spall strength increases from 0.9 to 1.1 GPa at 1.6-GPa impact stress to 1.3-GPa spall strength at 3.8-GPa impact stress and, upon further increase in the impact stress, it begins to decline (Figure 13). Its value (spall strength) at impact stress of 12 GPa is 0.82 GPa. The results of experiments 437 and 607 show that the spall strength of SiC-B at 2.6 GPa remains unchanged, even though the pulse widths in these experiments were 0.64 and 0.33  $\mu\text{s}$ , respectively. Extrapolation of the observed trend in spall strength of this material implies that it may not have measurable spall strength when shocked to 18 GPa. This needs to be confirmed through future experiments.

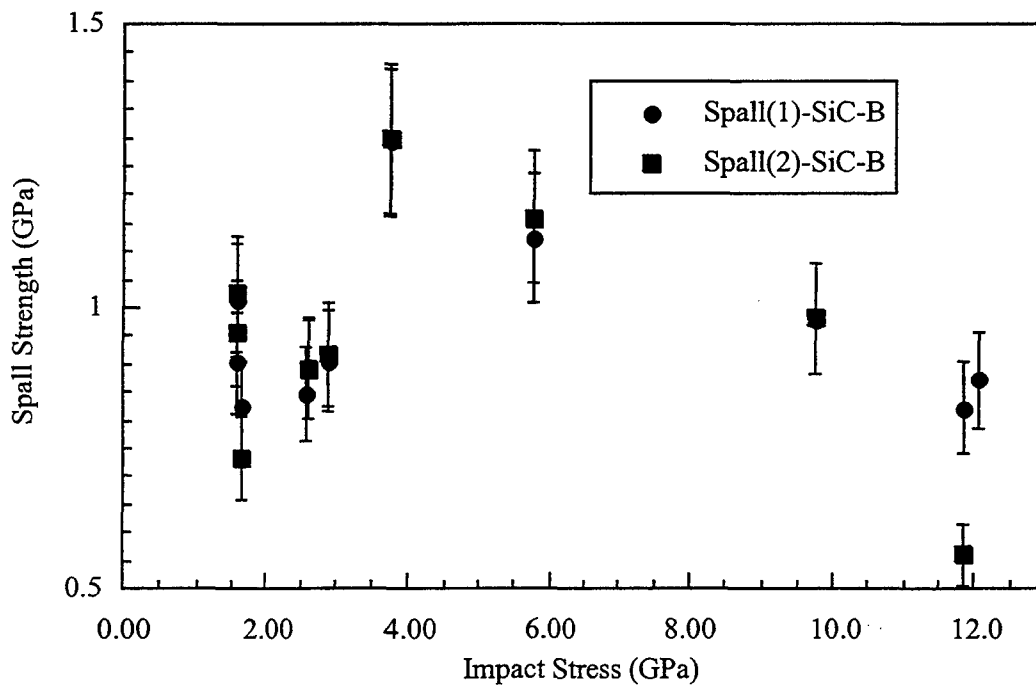


**Figure 13. Spall Strength vs. Impact Stress of SiC-B.**

5.2.2.2 *SiC-N*. Eleven experiments were conducted on SiC-N. The pulse width in eight of these experiments was 0.65  $\mu\text{s}$ . The variation in the value of spall strength with impact stress in SiC-N is shown in Figure 14. The pulse widths in experiments 607 and 617 were 0.71  $\mu\text{s}$  and the pulse width in experiment 636 was 0.35  $\mu\text{s}$ . The values of spall strength vary between 0.54 and

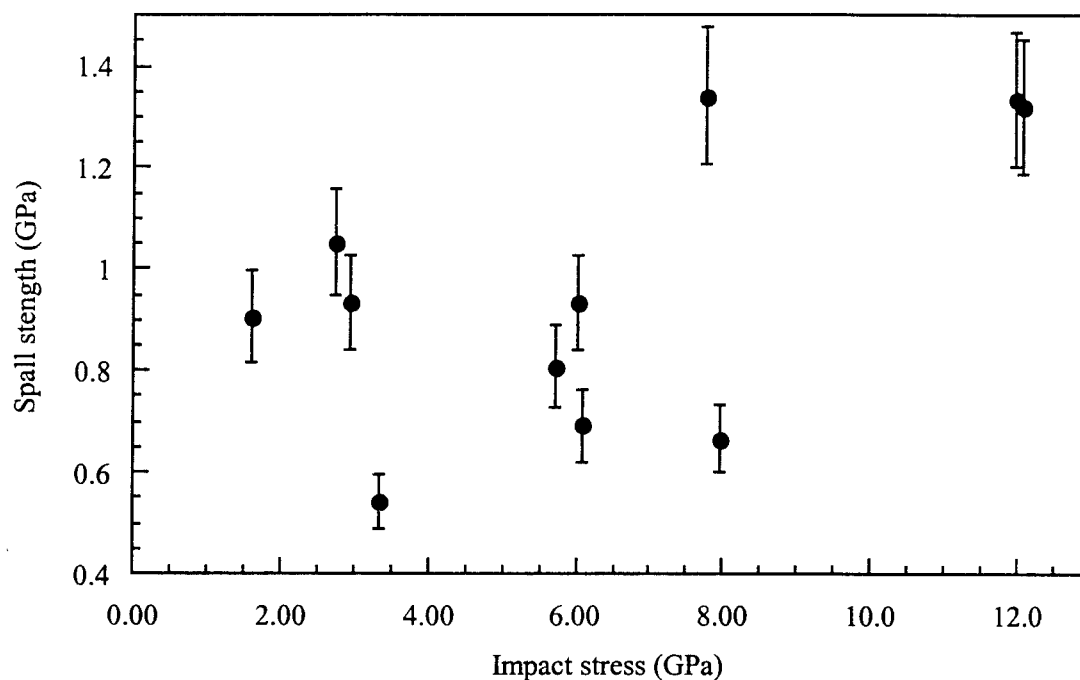


**Figure 14. Spall Strength vs. Impact Stress of SiC-N.**

1.3 GPa. However, there is no discernible trend in the variation of its spall strength values with the impact stress, as observed in the previous three materials. Further, there is a large scatter in the measured values of spall strength of this material. For example, the values of spall strength of SiC-N in three experiments (i.e., 617, 628, and 824-2 at impact stress around 6 GPa) are determined to be 0.69, 0.81, and 0.93 GPa, respectively. Whereas the pulse width in experiment 617 was 0.72  $\mu\text{s}$ , the pulse widths in the experiments 628 and 824-2 were 0.65 and 0.66  $\mu\text{s}$ , respectively. Similarly, the values of spall strength and associated pulse widths in three experiments performed at impact stresses between 2.7 and 3.3 GPa do not seem to follow any pattern. The spall strength and associated pulse width in these three experiments (namely, 519, 607, and 636) are 0.54 GPa, 0.65  $\mu\text{s}$ ; 1.05 GPa, 0.72  $\mu\text{s}$ ; and 0.93 GPa, 0.35  $\mu\text{s}$ , respectively. The wave profiles of these experiments are shown in Figure 15.

**5.2.3 French Sintered and Hot-Pressed SiC.** Five experiments were performed on this material, generating impact stresses between 1.5 and 16.8 GPa. The pulse widths in these

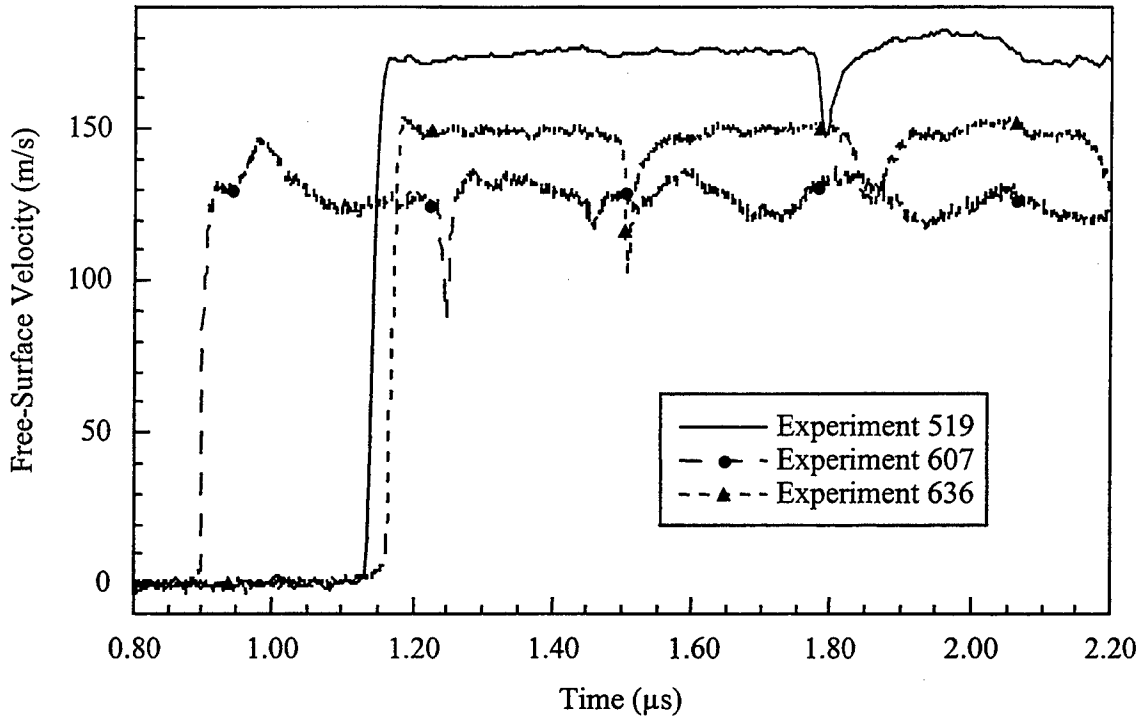


**Figure 15. Free-Surface Velocity Profiles in SiC-N.**

experiments varied between 0.58 and 0.67  $\mu\text{s}$ . The results of shock wave experiments on the French sintered and hot-pressed Sic are given in Tables 12 and 13. The values of spall strengths of the French sintered and hot-pressed material as a function of impact stress are plotted in Figure 16. The first feature one notices is the lack of scatter in the data compared to that observed in the other four Sic materials. Second, it shows that spall strength of this material continues to increase with an increase in the impact stress to 11.7 GPa and then shows a decline in its spall threshold at an impact stress of 16.8 GPa. Its spall strength at 16.8 GPa is determined to lie between 0.34 and 0.50 GPa. Figure 17 shows the free-surface velocity profiles in this material at impact stresses of 11.7 and 16.8 GPa. This large variation in the spall strength at 16.8 GPa is due to an observed deceleration in its free-surface velocity profile from a peak value of 0.863 km/s to 0.855/km/s (Figure 17). Thus, though these two values of the free-surface velocities are within 1% of each other, they lead to the aforementioned magnitudes of spall strength at 16.8 GPa. However, such a slowing down of free-surface velocity is not seen in any other experiments performed on this material. Irrespective of the origin of this deceleration, it is

**Table 12. Data From Transmission Experiments on French Sintered and Hot-Pressed SiC**

Experiment	Thickness (mm)		Impact Velocity (km/s)	Pulse Width ( $\mu$ s)	Free-Surface Velocity (km/s)		
	Flyer	Target			Shock	Spall	Recompression
520	4.013	7.99	0.6046	0.659	0.6118	0.5160	0.6126
522	3.99	8.003	0.0809	0.655	0.0813	0.0400	0.0831
525	3.972	7.998	0.401	0.652	0.4067	0.3415	0.4041
820 (WC)	2.029	6.011	0.5865	0.576	0.8630	0.8370	0.8558
820 (WC)	2.029	6.011	0.5865	0.576	0.8546	0.8370	0.8558
822 (FS/SiC)	4.025	6.014	0.2059	0.668	0.2062	0.1553	0.2044-0.1998
822 (FS/SiC)	4.025	6.014	0.2059	0.668	0.2010	0.1553	0.2044-0.1998

**Table 13. Summary of the Results of Transmission Experiments on French Sintered and Hot-Pressed SiC**

Experiment	Impact Velocity (km/s)	Shock State		Release Impedance ( $Gg/m^2 \cdot s$ )	Spall Strength	
		Mass Velocity (km/s)	Stress (GPa)		1/2 Pull-Back Change (km/s)	Stress (GPa)
520	0.6046	0.3023	11.729	37.90	0.0479	1.858
522	0.0809	0.0405	1.569	38.42	0.0207	0.801
525	0.401	0.2005	7.779	37.73	0.0326	1.265
820 (WC)	0.5865	0.4330	16.802	39.08	0.0130	0.504
820 (WC)	0.5865	0.4330	16.802	41.78	0.0088	0.341
822 (FS/SiC)	0.2059	0.1016	3.943	37.71	0.0254	0.987
822 (FS/SiC)	0.2059	0.1016	3.943	39.68	0.0228	0.887

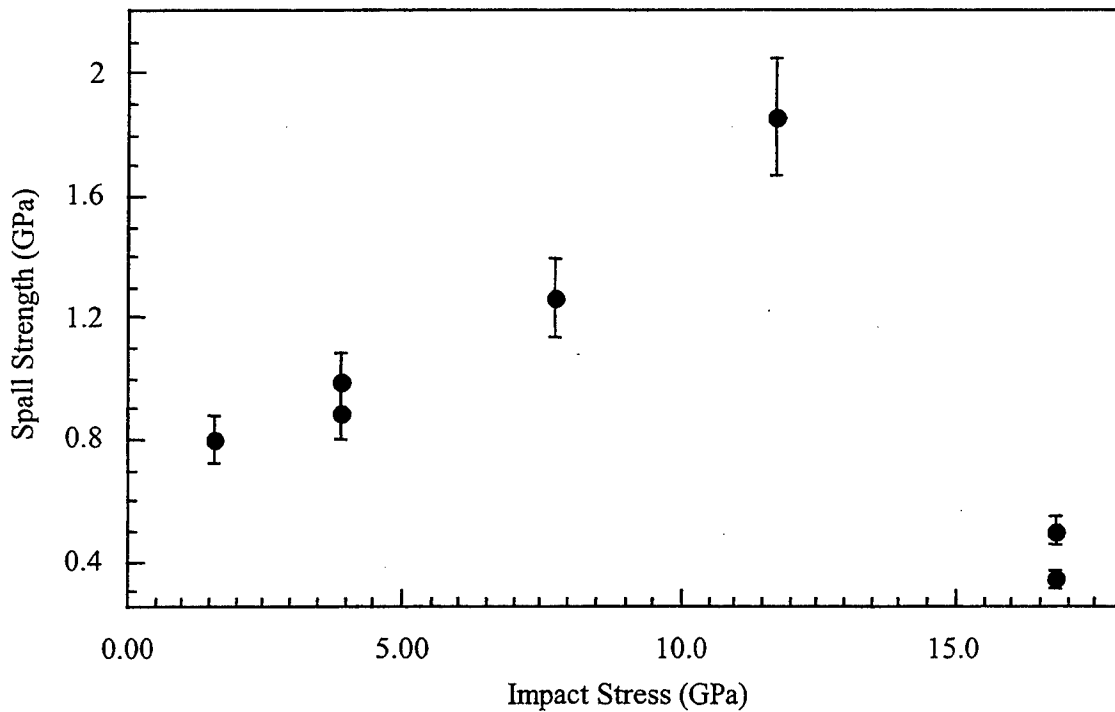


**Figure 16. Spall Strength vs. Impact Stress of French Sintered and Hot-Pressed SiC.**

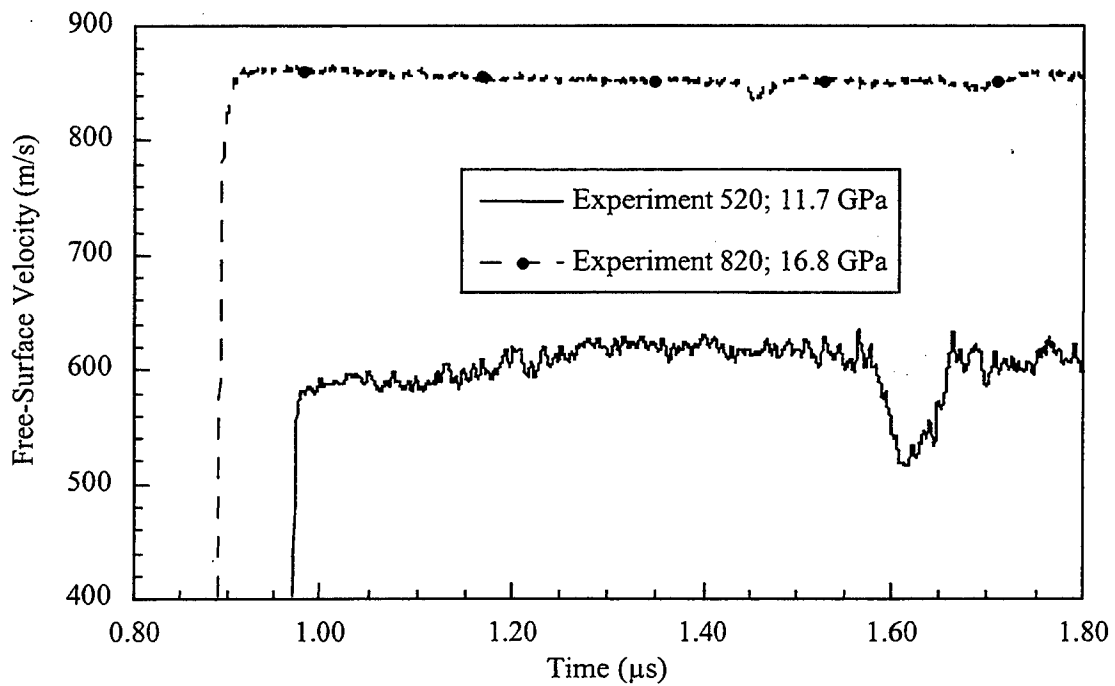


**Figure 17. Free-Surface Velocity Profiles in French Sintered and Hot-Pressed SiC.**

clear that spall threshold value drops precipitously when this material is shocked between 11.7 and 16.8 GPa. The increase in the value of spall threshold from 0.80 GPa at an impact stress of 1.6, to 1.85 GPa at an impact stress of 11.7 GPa, is impressive and unprecedented for a ceramic material.

**5.2.4 Summary.** The results of the experiments on five types of SiC may be summarized as follows.

**5.2.4.1 Spall Strength Variation Trend.** The trend in the variation of spall strength with impact stress in sintered (Sohio and French), SiC-B, and French sintered and hot-pressed materials show similarities. Spall strengths of these four materials appear to peak at some specific impact stress and then decline when the specific impact stress is exceeded. Thus, spall threshold in the first three materials increases until an impact stress between 3.7 and 5 GPa is reached, and then they begin to decline. For French sintered and hot-pressed material, the spall threshold increases up to an impact stress of 11.7 GPa and then begins to decline at higher impact stresses. SiC-N does not show such an unambiguous trend in the variation of its spall threshold with impact stress.

**5.2.4.2 Sohio Material.** Sohio material has relatively higher spall threshold than French sintered material. In general, hot-pressed materials, including the French material, which was both sintered and hot pressed, show a higher value of spall threshold than the materials that are sintered but not hot pressed. For instance, SiC-B has a spall strength of 0.90 GPa at an impact stress of 1.6 GPa, then peaks with a spall strength of 1.3 GPa at an impact stress of 3.75 GPa. Between an impact stress of 3.75 and 12.1 GPa, the spall strength declines to 0.90 GPa. Sohio SiC exhibits similar behavior, having spall strengths of 0.65, 0.95, and 0.40 GPa at impact stresses of 1.6, 3.6, and 11.5 GPa, respectively. The spall strength of French sintered material is 0.5 GPa at an impact stress 1.5 GPa and goes through a maximum value a of 0.63 GPa between 3.5–5.8 GPa. Upon further increase in impact stress, the spall strength decreases to 0.5 GPa at an impact stress of 11.5 GPa. In the case of the French sintered and hot-pressed material, spall

threshold value continues to increase from 0.8 GPa at 1.6 GPa to 1.8 GPa at an impact stress of 11.7 GPa. Its value decreases to 0.3–0.5 GPa at an impact stress of 16.8 GPa.

*5.2.4.3 Spall Threshold Increase.* The unprecedented increase in the spall threshold observed in the French sintered and hot-pressed SiC with an increase in impact stress is unique.

*5.2.4.4 Free-Surface Velocity Decline.* The gradual decline in the recorded free-surface velocity at 16.8 GPa in the French sintered and hot-pressed material suggests an increase in its mechanical impedance. Whether this is significant or not is an open question.

## 6. Discussion

Spall strength of a ceramic is generally a time-dependent process; it is always fracture initiated and dominated. Polycrystalline ceramic invariably contains impurities and micropore sites. It may also contain glassy phase or phases dispersed throughout its bulk. These sites and phases are favorable locations for the nucleation and growth of microcracks or microfissures during the propagation of shock waves. Possibly, release wave propagation also contributes to this growth. The number of microfractures generated will be sensitive to the number of these sites and the extent of glassy phase in the material, as well as duration of shock compressive pulse and its magnitude. This implies that, if nucleation and growth of microcracks in the material are time dependent at a given magnitude of shock-induced stress, then its spall strength will be pulse dependent. If, on the other hand, nucleation and growth of microcracks in the material are dependent on the magnitude of impact stress only, then its spall strength will not be influenced by the time duration of the shock. Since SiC materials that were unambiguously from the location undergoing the uniaxial strain changes in the wave propagation direction were unable to be recovered, it is not yet possible to ascertain a specific factor responsible for the spall values obtained on the five SiC investigated here. However, if the variability in the magnitudes of spall thresholds at a given stress with a specific value of pulse width exceeds the precision of the measurements, then it can be attributed to variation in the quality of the samples. Under the

attributed to variation in the quality of the samples. Under the aforementioned condition, depending on the generated population of microfractures, the spall strength of the material could be foreseen to vary significantly under shock-induced tension.

Both sintered materials show an initial increase in their spall strengths to 3–5 GPa and decline when shocked to higher stresses. The initial value of spall strength of Sohio material is higher than of French sintered material. The role of microstructure in the observed increase in the values of their respective spall strengths is unclear and lacks an explanation. The decrease in the spall strength with an increase in the impact stress is understandable in view of generation and extension of microcracks under shock and release. Earlier investigations on titanium diboride by Dandekar (1992, 1994a), Dandekar and Benfanti (1993), Ewart and Dandekar (1994), and Winkler and Stilp (1992a) showed that its spall strength decreased with an increase in the impact stress. Further studies to probe the nature of the first cusp observed in titanium diboride around 4–6 GPa found it to be associated with its elastic deformation. As a consequence, its spall strength under single shock and release, and under repeated shock and release below the first cusp, remained constant around 0.35 GPa. However, when titanium diboride was shocked to 6.8 GPa, beyond the first cusp level, its spall strength under single shock and release reduced to 0.18 GPa. Spall strength under repeated shock and release was decreased to 0.07 GPa. The microstructural studies of the recovered titanium diboride materials by Ewart and Dandekar (1994) showed that defects generated during the shock wave experiments were responsible for the observed decrease in its spall strength. Winkler and Stilp (1992a) came to similar conclusions from their investigation on titanium diboride. None of the SiC material investigated in this work show a first cusp in their wave profile as observed in titanium diboride. Yet, only repeated shock-release experiments, as done earlier on titanium diboride (Dandekar and Benfanti 1993), combined with careful microstructural examination of shock-recovered materials can lead to understanding the observed initial increase in the spall strengths of these materials with an increase in the impact stress.

The spall strength of SiC-B shows a trend similar to those shown by the two sintered silicon carbide materials. An increase in its spall strength is observed up to around 3 GPa, and when shocked beyond this stress level, the spall strength begins to decline. The spall strength of SiC-N does not show an unambiguous trend in the variation of its spall strength with impact stress. The scatter in the experimental data is very puzzling. The best guess is that observed scatter in the data is probably because SiC-N material quality varied widely. The highest value of spall strength 1.32–1.34 GPa is obtained at impact stress between 8 and 12 GPa.

The spall strength of French sintered and hot-pressed SiC shows very little scatter in the data. Spall strength increases from around 0.8 GPa at an impact stress of 1.6 GPa to 1.86 GPa when shocked to 11.7 GPa. When shocked to 16.8 GPa, the spall threshold reduces to 0.3–0.5 GPa. In an earlier investigation on a hot-pressed SiC, Winkler and Stilp (1992b) also found the spall strength of their material increasing with an increase in the impact stress. The data from their experiments on SiC is plotted in Figure 18. It shows that the spall strength of hot-pressed SiC increases from 0.6 GPa at an impact stress of 0.7 GPa to 1.1 GPa at 11.4 GPa and then begins to decline, with a value of 0.7 GPa at an impact stress of 20 GPa. The flyers used by Winkler and Stilp in these experiments are as follows: for 0.7-GPa experiment, a 0.7-mm-thick PMMA was used; for 1.3-GPa impact stress experiment, a 1.6-mm-thick aluminum flyer was used; the remaining experiments use an Armco iron flyer, with either 1-mm or 1.6-mm thickness. SiC targets were 5.5–6 mm thick. Winkler and Stilp (1992b) report the HEL of their SiC to be between 13 and 14.7 GPa. Since they do not report the errors associated with their measurements of spall strength, it is difficult to state whether or not the difference in the values of the spall thresholds 0.5 and 0.7 GPa at impact stresses 12 and 20 GPa, respectively, are significantly different from one another.

In the present experiments, the variation of spall strength with impact stress in SiC does not exhibit behavior similar to other ceramics. For example, titanium diboride has a spall strength that is constant at 0.33 GPa up to an impact stress of 5.9 GPa. Above 5.9 GPa, the spall strength decreases to nearly 0 at its HEL of 13.5 GPa. On the other hand, Coors AD995

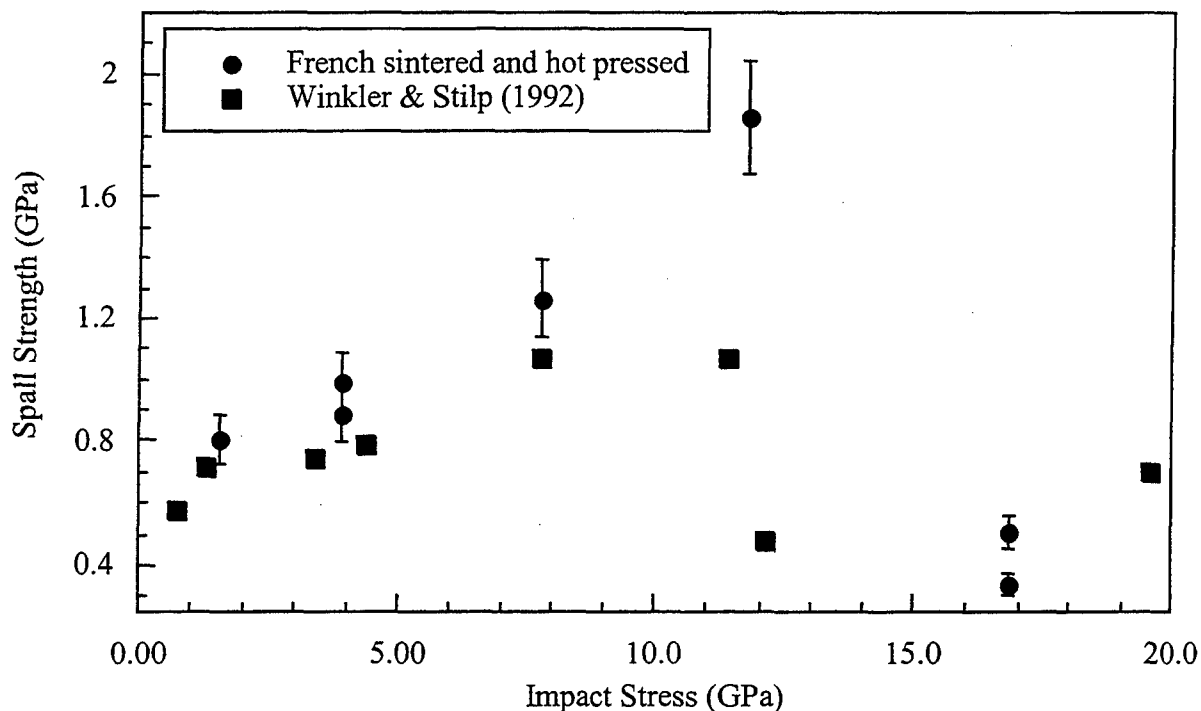


**Figure 18. Spall Strength vs. Impact Stress of French Sintered and Hot-Isostatically-Pressed SiC and Hot-Pressed SiC, From Winkler and Stilp (1992b).**

alumina has a constant spall threshold of 0.45 GPa beyond its HEL of 6.7 GPa. The rate of growth of defects increases with duration of impact stress in AD995, evident by the decrease in spall strength with increase in impact stress pulse width.

## 7. Future Work

The single most important result of this investigation is that spall strength of SiC, irrespective of its manufacturing process, improves initially to a certain impact stress level before it begins to deteriorate under higher impact stress. In terms of spall strength, the French sintered and hot-pressed material shows least scatter and largest increase with an increase in the impact stress. In view of the aforementioned, it will be very useful to conduct spall experiments subjected to repeated shock and release, as done earlier on titanium diboride (Dandekar and Benfanti 1993)

combined with careful microstructural examination of shock recovered materials to understand the observed initial increase in the spall strengths of these materials with an increase in the impact stress.

INTENTIONALLY LEFT BLANK.

## 8. References

- Barker, L. M., and R. E. Hollenbach. "Laser Interferometer for Measuring High Velocities of Any Reflecting Surface." *Journal of Applied Physics*, vol. 43, pp. 4669–4680, 1972.
- Bartkowski, P., and D. P. Dandekar. "Spall Strengths of Sintered and Hot Pressed SiC." *Shock Compression of Condensed Matter-1995*, pp. 535–539, S. C. Schmidt and W. C. Tao (editors), American Institute of Physics, New York, NY, 1996.
- Bartkowski, P., and D. P. Dandekar. "Effects of PMMA Hugoniot on Calculated Spall Strength of AD995 Alumina." Presented at 1997 Topical Conference on Shock Compression of Condensed Matter, 27 July–1 August 1997, Amherst, MA, 1997.
- Bartkowski, P., and D. P. Dandekar. Unpublished data. 1999.
- Belayt, L., and C. E. Cottenot. "Post-Mortem Microstructural Characterization of SiC Materials After Interaction With a Kinetic Energy Projectile." *Structures Under Shock and Impact IV*, pp. 459–468, N. Jones, C. A. Brebia, and A. J. Watson (editors), Computational Mechanics Publications, Boston, MA, 1996.
- Dandekar, D. P. "Effect of Shock-Re-Shock on Spallation of Titanium Diboride." *Shock Compression of Condensed Matter-1991*, pp. 487–490, S. C. Schmidt, R. D. Dick, J. W. Forbes, and D. G. Tasker (editors), Elsevier, Amsterdam, 1992.
- Dandekar, D. P. "Response of Ceramics Under Shock-Wave Loading." *High-Pressure Science and Technology-1993*, pp. 729–732, S. C. Schmidt, J. W. Shaner, G. A. Samara, and M. Ross (editors), American Institute of Physics, New York, NY, 1994a.
- Dandekar, D. P. "Response of Protective Ceramics Under Single and Multiple Impacts." *Wave Propagation and Emerging Technologies*, AMD vol. 188, pp. 133–141, V. K. Kinra, R. J. Clifton, and G. C. Johnson (editors), New York, NY: ASME Press, 1994b.
- Dandekar, D. P. "Experimental Technique to Measure Tensile Impedance of a Material Under Plane Shock Wave Propagation." *Shock Compression of Condensed Matter-1995*, pp. 947–950, S. C. Schmidt, and W. C. Tao (editors), American Institute of Physics, New York, NY, 1996.
- Dandekar, D. P., and P. Bartkowski. "Shock Response of AD995 Alumina." *High-Pressure Science and Technology-1993*, pp. 733–736, S. C. Schmidt, J. W. Shaner, G. A. Samara, and M. Ross (editors), American Institute of Physics, New York, NY, 1994.

- Dandekar, D. P., and D. C. Benfanti. "Strength of Titanium Diboride Under Shock Wave Loading." *Journal of Applied Physics*, vol. 73, pp. 673-679, 1993.
- Dandekar, D. P., P. J. Gaeta, and Y. Horie. "Double Shock and Release Experiments in PMMA and Z-Cut Sapphire." *Shock Compression in Condensed Matter-1987*, pp. 281-284, S. C. Schmidt and N. C. Holms (editors), Elsevier, Amsterdam, 1988.
- Ewart, L., and D. P. Dandekar. "Relationship Between The Shock Response and Microstructural Features of Titanium Diboride (TiB<sub>2</sub>)." *High-Pressure Science and Technology-1993*, pp. 1201-1204, S. C. Schmidt, J. W. Shaner, G. A. Samara, and M. Ross (editors), American Institute of Physics, New York, NY, 1994.
- Papadakis, E. P. "Ultrasonic Phase Velocity by the Pulse-Echo-Overlap Method Incorporating Diffraction Phase Corrections." *Journal of Acoustic Society of America*, vol. 40 pp. 1045-1051, 1967.
- Shih, J. "Dynamic Deformation of SiC." Doctoral Thesis, University of California, San Diego, CA, 1998.
- Winkler, W. T., and A. J. Stilp. "Pressure Induced Macro- and Micromechanical Phenomena in Planar Impacted TiB<sub>2</sub>." *Shock Compression of Condensed Matter-1991*, pp. 555-558, S. C. Schmidt, R. D. Dick, J. W. Forbes, and D. G. Tasker (editors), Elsevier, Amsterdam, 1992a.
- Winkler, W. T., and A. J. Stilp. "Spallation Behavior of TiB<sub>2</sub>, SiC, and B<sub>4</sub>C Under Planar Impact Stresses." *Shock Compression of Condensed Matter-1991*, pp. 475-478, S. C. Schmidt, R. D. Dick, J. W. Forbes, and D. G. Tasker (editors), Elsevier, Amsterdam, 1992b.

<u>NO. OF COPIES</u>	<u>ORGANIZATION</u>
2	DEFENSE TECHNICAL INFORMATION CENTER DTIC DDA 8725 JOHN J KINGMAN RD STE 0944 FT BELVOIR VA 22060-6218
1	HQDA DAMO FDT 400 ARMY PENTAGON WASHINGTON DC 20310-0460
1	OSD OUSD(A&T)/ODDDR&E(R) R J TREW THE PENTAGON WASHINGTON DC 20301-7100
1	DPTY CG FOR RDA US ARMY MATERIEL CMD AMCRDA 5001 EISENHOWER AVE ALEXANDRIA VA 22333-0001
1	INST FOR ADVNCD TCHNLGY THE UNIV OF TEXAS AT AUSTIN PO BOX 202797 AUSTIN TX 78720-2797
1	DARPA B KASPAR 3701 N FAIRFAX DR ARLINGTON VA 22203-1714
1	US MILITARY ACADEMY MATH SCI CTR OF EXCELLENCE MADN MATH MAJ HUBER THAYER HALL WEST POINT NY 10996-1786
1	DIRECTOR US ARMY RESEARCH LAB AMSRL D D R SMITH 2800 POWDER MILL RD ADELPHI MD 20783-1197

<u>NO. OF COPIES</u>	<u>ORGANIZATION</u>
1	DIRECTOR US ARMY RESEARCH LAB AMSRL DD 2800 POWDER MILL RD ADELPHI MD 20783-1197
1	DIRECTOR US ARMY RESEARCH LAB AMSRL CI AI R (RECORDS MGMT) 2800 POWDER MILL RD ADELPHI MD 20783-1145
3	DIRECTOR US ARMY RESEARCH LAB AMSRL CI LL 2800 POWDER MILL RD ADELPHI MD 20783-1145
1	DIRECTOR US ARMY RESEARCH LAB AMSRL CI AP 2800 POWDER MILL RD ADELPHI MD 20783-1197
	<u>ABERDEEN PROVING GROUND</u>
4	DIR USARL AMSRL CI LP (BLDG 305)

<u>NO. OF COPIES</u>	<u>ORGANIZATION</u>	<u>NO. OF COPIES</u>	<u>ORGANIZATION</u>
1	CECOM SP & TRRSTRL COMMCTN DIV AMSEL RD ST MC M H SOICHER FT MONMOUTH NJ 07703-5203	1	DARPA L STOTTS 3701 N FAIRFAX DR ARLINGTON VA 22203-1714
1	PRIN DPTY FOR TCHNLGY HQ US ARMY MATCOM AMCDCGT R PRICE 5001 EISENHOWER AVE ALEXANDRIA VA 22333-0001	1	DIRECTOR US ARMY RESEARCH LAB AMSRL CS AL TA 2800 POWDER MILL ROAD ADELPHI MD 20783-1145
1	PRIN DPTY FOR ACQUSTN HQS US ARMY MATCOM AMCDCGA D ADAMS 5001 EISENHOWER AVE ALEXANDRIA VA 22333-00001	3	DIRECTOR US ARMY ARDEC AMSTA AR FSA E W P DUNN J PEARSON E BAKER PICATINNY ARSENAL NJ 07806-5000
1	DPTY CG FOR RDE HQS US ARMY MATCOM AMCRD 5001 EISENHOWER AVE ALEXANDRIA VA 22333-00001	2	US ARMY TARDEC K BISHNOI D TEMPLETON AMSTRA TR R MS 263 WARREN MI 48397-5000
1	ASST DPTY CG FOR RDE HQS US ARMY MATCOM AMCRD COL S MANESS 5001 EISENHOWER AVE ALEXANDRIA VA 22333-00001	4	COMMANDER US ARMY BELVOIR RD&E CTR STRBE N WESTLICH STRBE NAN S G BISHOP J WILLIAMS FORT BELVOIR VA 22060-5166
3	AIR FORCE ARMAMENT LAB AFATL DLJW W COOK D BELK J FOSTER ELGIN AFB FL 32542	1	COMMANDER US ARMY RESEARCH OFFICE A RAJENDRAN PO BOX 12211 RESEARCH TRIANGLE PARK NC 27709-2211
1	DPTY ASSIST SCY FOR R & T SARD TT THE PENTAGON RM 3E479 WASHINGTON DC 20310-0103	1	NAVAL RESEARCH LAB A E WILLIAMS CODE 6684 4555 OVERLOOK AVE SW WASHINGTON DC 20375

<u>NO. OF COPIES</u>	<u>ORGANIZATION</u>	<u>NO. OF COPIES</u>	<u>ORGANIZATION</u>
10	DIRECTOR SANDIA NATL LABS E S HERTEL JR MS 0819 J ASAY MS 1811 R BRANNON MS 0820 L CHHABILDAS MS 1811 D CRAWFORD MS 0821 M FURNISH MS 0821 P TAYLOR ORG 1432 M KIPP MS 0820 P YARRINGTON MS 0820 M FORRESTAL DIV 1551 PO BOX 5800 ALBUQRQUE NM 87185-0307	1	ARMY HIGH PERFORMANCE COMPUTING RSRCH CTR T HOLMQUIST 1200 WASHINGTON AVENUE S MINNEAPOLIS MN 55415
		2	SOUTHWEST RESEARCH INSTITUTE C ANDERSON J WALKER P O DRAWER 28510 SAN ANTONIO TX 78284
		2	UNIVERSITY OF DELAWARE DEPT OF MECH ENGINEERING PROF J GILLESPIE PROF J VINSON NEWARK DE 19716
10	DIRECTOR LLNL M J MURPHY J AKELLA N C HOLMES W TAO L282 J FORBES P URTIEW L282 A HOLT L290 J E REAUGH L290 W J NELLIS L299 J B CHASE L099 PO BOX 808 LIVERMORE CA 94550	3	SRI INTERNATIONAL D CURRAN D SHOCKEY R KLOPP 333 RAVENSWOOD AVENUE MENLO PARK CA 94025
		1	VIRGINIA POLYTECHNIC INST COLLEGE OF ENGINEERING R BATRA BLACKSBURG VA 24061-0219
7	DIRECTOR LANL D MANDELL P MAUDLIN R GRAY J SHANER MS F670 R DAVIDSON MS K557 J JOHNSON G787 F ADDESSIO G787 PO BOX 1663 LOS ALAMOS NM 87545	1	ALLIANT TECHSYSTEMS INC GR JOHNSON MN11 1614 600 SECOND ST NE HOPKINS MN 55343
		1	COMPUTATIONAL MECHANICS CONSULTANTS J A ZUKAS P O BOX 11314 BALTIMORE MD 21239-0314
3	CALTECH A INGERSOLL MS 170 25 PROF G RAVICHANDRAN T J AHRENS MS 252 21 1201 E CALIFORNIA BLVD PASADENA CA 91125	1	KAMAN SCIENCES CORP D L JONES 2560 HUNTINGTON AVE SUITE 200 ALEXANDRIA VA 22303

NO. OF COPIES	ORGANIZATION
9	INST OF ADVANCED TECHNOLOGY UNIVERSITY OF TX AUSTIN S BLESS J CAZAMIAS H FAIR D LITTLEFIELD I MCNAB C PERSAD W REINECKE P SULLIVAN S SATAPATHY 3925 W BRAKER LANE SUITE 400 AUSTIN TX 78759-5316
1	APPLIED RESEARCH ASSOCIATES D E GRADY 4300 SAN MATEO BLVD NE SUITE A220 ALBUQUERQUE NM 87110
1	INTERNATIONAL RESEARCH ASSOCIATES INC D L ORPHAL 4450 BLACK AVE PLEASANTON CA 94566
1	JET PROPULSION LABORATORY M ADAMS IMPACT PHYSICS GROUP 4800 OAK GROVE DRIVE PASADENA CA 91109
1	THE DOW CHEMICAL CO M EL RAHEB CENTRAL RSRCH ENGINEERING LABORATORY BUILDING 1776 MIDLAND MI 48640
1	BOB SKAGGS CONSULTANT S R SKAGGS 79 COUNTY RD 117 SOUTH SANTA FE NM 87501
1	WASHINGTON ST UNIVERSITY SCHOOL OF MECHANICAL AND MATERIAL ENGINEERING J L DING PULLMAN WA 99164-2920

NO. OF COPIES	ORGANIZATION
1	WASHINGTON ST UNIVERSITY INSTITUTE OF SHOCK PHYSICS Y M GUPTA PULLMAN WA 99164-2814
1	COORS CERMANIC COMPANY T RILEY 600 NINTH STREET GOLDEN CO 80401
1	ARIZONA STATE UNIVERSITY MECHANICAL AND AEROSPACE ENGINEERING D KRAVCINOVIC TEMPE AZ 85287-6106
1	UNIVERSITY OF DAYTON RESEARCH INSTITUTE 300 COLLEGE PARK C HARI SIMHA MS SPC 1911 DAYTON OH 45469
5	DIRECTOR USARL K WILSON (5 CPS) FRENCH DEA 1396 ADELPHI MD 20783-1197
	<u>ABERDEEN PROVING GROUND</u>
39	DIRECTOR USARL AMSRL WM E SCHMIDT T WRIGHT AMSRL WM TA T HAVEL M NORMANDIA W A GOOCH P BARTKOWSKI (10) H W MEYER E HORWATH AMSRL WM TC K KIMSEY D SCHEFFLER R COATES AMSRL WM PD G GAZONAS AMSRL WM WD A PRAKASH

NO. OF  
COPIES    ORGANIZATION

AMSRL WM TD  
A M DIETRICH  
M RAFTENBERG  
M SCHEIDLER  
E RAPACKI  
J M BOTELER  
T WEERASOORIYA  
D GROVE  
D DANDEKAR (10)

<u>NO. OF COPIES</u>	<u>ORGANIZATION</u>	<u>NO. OF COPIES</u>	<u>ORGANIZATION</u>
1	DERA N J LYNCH WEAPONS SYSTEMS BUILDING A20 DRA FORT HALSTEAD SEVENOAKS KENT TN 147BP UNITED KINGDOM	1	ROYAL MILITARY COLLEGE OF SCIENCE CRANEFIELD UNIVERSITY PROF N BOURNE SHRIVENHAM SWINDON SN6 8LA UNITED KINGDOM
2	ERNST MACH INTITUT VOLKER HOHLER H NAHAME ECKERSTRASSE 4 D-7800 FREIBURG 1 BR 791 4 GERMANY		
1	FOA2 PATRIK LUNDBERG S-14725 TUMBA SWEDEN		
1	PCS GROUP CAVENDISH LABORATORY WILLIAM G PROUD MADINGLEY RD CAMBRIDGE UNITED KINGDOM		
1	CENTRE D'ETUDES DE GRAMAT J Y TRANCHET 46500 GRAMAT FRANCE		
1	MINISTERE DE LA DEFENSE DR G BRAULT DGA/DSP/STTC 4, RUE DE LA PORTE D'ISSY 75015 PARIS FRANCE		
1	SPART DIRECTION - BP 19 DR E WARINGHAM 10 PLACE GEORGES CLEMENCEUX 92211 SAINT CLOUD CEDEX FRANCE		

REPORT DOCUMENTATION PAGE			Form Approved OMB No. 0704-0188	
Public reporting burden for this collection of information is estimated to average 1 hour per response, including the time for reviewing instructions, searching existing data sources, gathering and maintaining the data needed, and completing and reviewing the collection of information. Send comments regarding this burden estimate or any other aspect of this collection of information, including suggestions for reducing this burden, to Washington Headquarters Services, Directorate for Information Operations and Reports, 1215 Jefferson Davis Highway, Suite 1204, Arlington, VA 22202-4302, and to the Office of Management and Budget, Paperwork Reduction Project(0704-0188), Washington, DC 20503.				
1. AGENCY USE ONLY (Leave blank)	2. REPORT DATE March 2001	3. REPORT TYPE AND DATES COVERED Final, October 1998 - September 1999		
4. TITLE AND SUBTITLE Tensile Strengths of Silicon Carbide (SiC) Under Shock Loading			5. FUNDING NUMBERS 0602105AH84	
6. AUTHOR(S) Dattatraya P. Dandekar and Peter T. Bartkowski				
7. PERFORMING ORGANIZATION NAME(S) AND ADDRESS(ES) U.S. Army Research Laboratory ATTN: AMSRL-WM-TD Aberdeen Proving Ground, MD 21005-5066			8. PERFORMING ORGANIZATION REPORT NUMBER ARL-TR-2430	
9. SPONSORING/MONITORING AGENCY NAMES(S) AND ADDRESS(ES)			10. SPONSORING/MONITORING AGENCY REPORT NUMBER	
11. SUPPLEMENTARY NOTES				
12a. DISTRIBUTION/AVAILABILITY STATEMENT  Approved for public release; distribution is unlimited.			12b. DISTRIBUTION CODE	
13. ABSTRACT (Maximum 200 words)  The present work was initiated to measure and compare tensile strengths (i.e., spall thresholds) of five different types/varieties of silicon carbide materials. Two of these materials were sintered, and the remaining three were hot-pressed. Three types of silicon carbides (one sintered by Sohio and the other two hot-pressed by Cercom) were manufactured in the United States. The remaining two varieties of silicon carbides were manufactured in France. Spall strengths of these five different silicon carbide materials were measured by performing plane shock wave experiments to a maximum impact-generated stress level of 17 GPa on the light gas-gun facility at the U.S. Army Research Laboratory (ARL). The single most important result of this investigation is that spall strength of silicon carbide, irrespective of its manufacturing process, improves initially to a certain impact stress level before it begins to deteriorate under higher impact stress. The decline in the spall strength of both sintered materials and Cercom SiC-B begin at an impact stress between 3-5 GPa. SiC-N data have a very large scatter. Spall strength of the French sintered and hot-pressed material increases to an impact stress of 11.7 GPa. Its spall strength increases from 0.8 GPa at an impact stress of 1.6 GPa to 1.8 GPa at an impact stress of 11.7 GPa. In terms of spall strength, the French sintered and hot-pressed materials show the least scatter and largest increase with an increase in the impact stress. The results of the present work thus offer new challenges to modeling ceramic materials.				
14. SUBJECT TERMS tensile strength, shock, silicon carbide, spall			15. NUMBER OF PAGES 49	
			16. PRICE CODE	
17. SECURITY CLASSIFICATION OF REPORT UNCLASSIFIED	18. SECURITY CLASSIFICATION OF THIS PAGE UNCLASSIFIED	19. SECURITY CLASSIFICATION OF ABSTRACT UNCLASSIFIED	20. LIMITATION OF ABSTRACT UL	

## ERRATA SHEET

re: ARL-TR-2430 "Tensile Strengths of Silicon Carbide (SiC) Under Shock Loading,"  
March 2001,  
by Dattatraya P. Dandekar and Peter T. Bartkowski

Replace page 26 with the new page 26 enclosed – Figure 14 was incorrect in the printed report.

20010402116

A388072